Contract No:

This document was prepared in conjunction with work accomplished under Contract No. 89303321CEM000080 with the U.S. Department of Energy (DOE) Office of Environmental Management (EM).

Disclaimer:

We put science to work.™

Savannah River National Laboratory™

OPERATED BY SAVANNAH RIVER NUCLEAR SOLUTIONS

A U.S. DEPARTMENT OF ENERGY NATIONAL LABORATORY • SAVANNAH RIVER SITE • AIKEN, SC

Waste Control Specialists Technical Review Team Report

November 2022

SRNL-RP-2022-00643
Revision 0

SRNL.DOE.GOV

DISCLAIMER

Printed in the United States of America

Prepared for
U.S. Department of Energy

SRNL-RP-2022-00643
Rev. 0

Keywords: Los Alamos National Laboratory, LANL, transuranic, TRU, drum, Waste Control Specialists, WCS, RNS

Retention: *Permanent*

Waste Control Specialists Technical Review Team Report

November 2022

APPROVALS

Waste Control Specialists (WCS) Technical Review Team (TRT)
National Laboratory Leads

_____

Audrey M. Williams Date
Lawrence Livermore National Laboratory

_____

Phillip F. Britt Date
Oak Ridge National Laboratory

_____

Michael J. Minnette Date
Pacific Northwest National Laboratory

_____

Michael L. Hobbs Date
Sandia National Laboratory

_____

Frank M. Pennebaker Date
Savannah River National Laboratory

Acknowledgements

We would like to acknowledge all of the team members for their time, technical expertise, and perseverance in seeing this report to completion. Mike Hobbs, Michael Kaneshige,and David Rosenberg of Sandia National Laboratory; Phillip Britt of Oak Ridge National Laboratory; Jon Schwantes and Michael Minette of Pacific Northwest National Laboratory; Audrey Williams and Jessica Mintz of Lawrence Livermore National Laboratory; Frank Pennebaker and Bob Pierce of Savannah River National Laboratory; and David Hobbs, an independent contractor.

We want to thank Kerry Watson (DOE Carlsbad Field Office) and Mark Pearcy (WIPP) for providing the repository temperatures. An extra thanks to Kerry Watson for providing an updated graphic of the MCC configuration image and valuable perspectives.

We are grateful for the assistance of Doug Ammerman (SNL), Ryan Williams (WCS), and Dave Nickless (DOE Environmental Management Los Alamos Field Office) for providing the MCC data.

We want to acknowledge the assistance of Davis Christensen (LANL) for operational information about the remediation of the nitrate salt waste.

We sincerely appreciate SNL internal reviewers Bill Erikson and Alex Brown and PNNL internal reviewer Judith Bamberger.

Summary / Key Judgments

1. Modeling of Drum 68660 and the WCS Drums: A calibrated model of Los Alamos National Laboratory (LANL) Drum 68660 indicates that pressurization of the drum by restriction of drum venting could have led to the thermal runaway reaction at the Waste Isolation Pilot Plant (WIPP) in 2014, supporting the hypothesis that the contents of the drum were not fundamentally different from the overall remediated nitrate salt (RNS) waste stream.

2. Nitric Acid Reactions and Aging of the Waste: The stability of the WCS RNS waste with respect to autocatalytic thermal runaway due to nitric acid chemistry should increase over time as the nitric acid is depleted from chemical reactions in the drum. However, this cannot be confirmed because of the lack of long-term experimental data on the impact of aging on the reactivity of RNS waste. The calibrated model indicates that the waste drums retain most of their reactive components, metal nitrate salts and sWheat Scoop®, even after eight years.

3. Pressure Effects and Runaway Reactions: The calibrated model indicates that if the drums and standard waste boxes (SWBs) are not allowed to pressurize during transport or storage and they are stored at historical WIPP repository temperatures, then an autocatalytic thermal runaway event is not expected to occur. Since the cause of Drum 68660 pressurization is not known, decision makers are not able to tailor mitigating strategies to the initiating event. Consequently, mitigating strategies must consider all feasible internal and external events that could lead to the pressurization of the drums.

4. Temperature Effects and Runaway Reactions: Temperature also has a strong influence on the stability of the waste. The calibrated model indicates that cooling the drums or SWBs can reduce the possibility of autocatalytic thermal runaway reactions. Simulations suggest that for a drum with a plugged vent, the probability of thermal runaway may be reduced or eliminated if wastes are maintained at or below 43 °F through active cooling measures from the initiation of transport until emplacement at WIPP.

Note: Any subjective views or opinions that might be expressed in this paper do not necessarily represent the views of the U.S. Department of Energy (DOE) or the United States Government.

Table of Contents

Acronyms and Abbreviations

ARC	accelerating rate calorimeter
CSB	container storage building
DOE	Department of Energy
LANL	Los Alamos National Laboratory
LHS	Latin hypercube sampling
MCC	Modular Concrete Canister
PNNL	Pacific Northwest National Laboratory
POC	pipe overpack container
PVC	polyvinylchloride
RNS	Remediated nitrate salt
SITI	Sandia Instrumented Thermal Ignition
SNL	Sandia National Laboratories
SRNL	Savannah River National Laboratory
SWB	Standard waste box
TRT	Technical Review Team
TRU	transuranic
WB8	Weisbrod 8 unremediated nitrate salt surrogate
WCS	Waste Control Specialists LLC
WIPP	Waste Isolation Pilot Plant

1.0 Description of the Waste Drums

The remediated nitrate salt (RNS) drums presently stored at the Waste Control Specialists (WCS) site near Andrews, Texas were produced at Los Alamos National Laboratory (LANL) between August 14, 2013, and March 18, 2014. The RNS drums contain moist acidic nitrate salts (from nitric acid processing of plutonium) mixed with sWheat Scoop® and, in some cases, neutralized acidic liquids absorbed onto sWheat, and job control waste. Between one and four RNS drums were placed inside each standard waste box (SWB), prior to shipment to the WCS site. The population of RNS drums contains 113 Type 3[1] drums and includes RNS packaged in 32 pipe overpack containers (POC) inside drums. The POCs were used to provide additional shielding of wastes with elevated dose rates. Figure 1-1 shows the configuration of the drums and SWBs inside the MCCs.

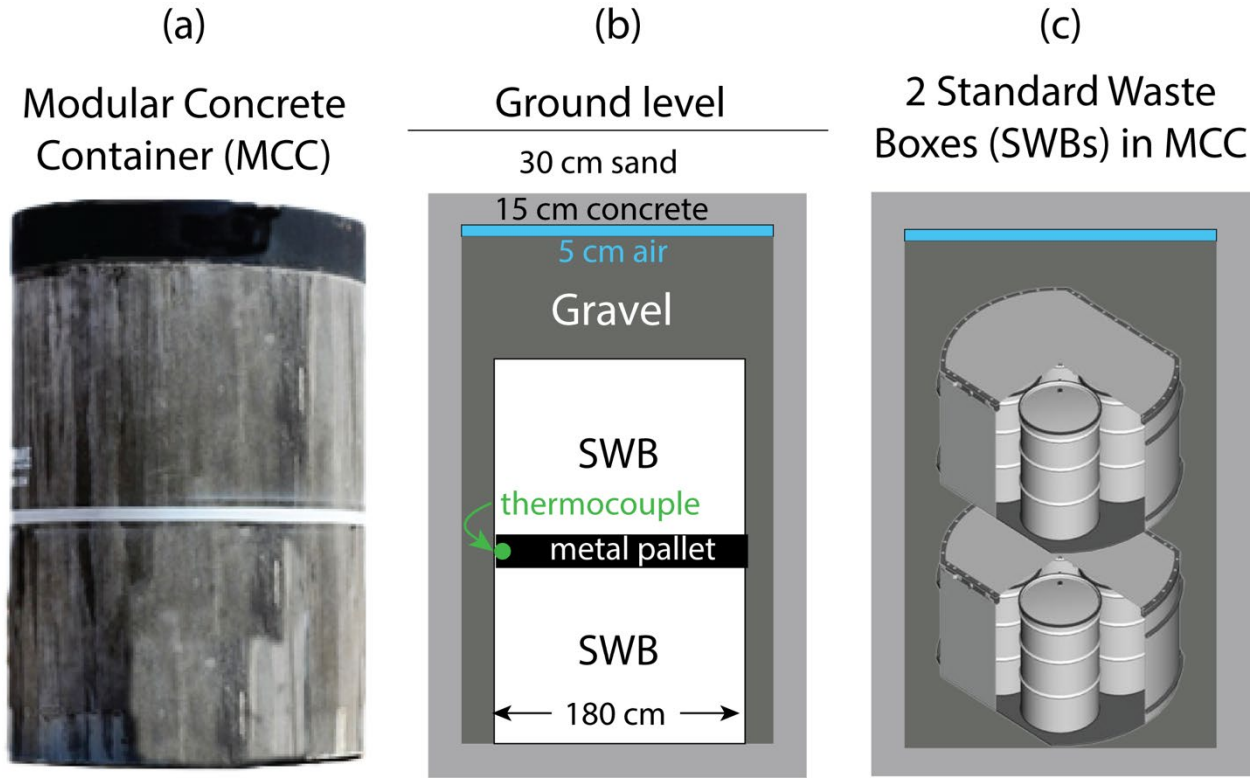

Figure 1-1. (a) Picture of MCC, (b) internals of MCC showing SWBs and thermocouple, (c) placement of 2 SWBs in MCC. SWBs have capacity to contain four drums. In most cases, SWBs contain only one drum with RNS, although some SWBs contain two drums with RNS.

After the event with Drum 68660 at the Waste Isolation Pilot Plant (WIPP), no other drums were shipped to WIPP. Instead, RNS drums were loaded into SWBs along with dunnage and other TRU waste drums and shipped from LANL to WCS, beginning April 1, 2014. Shipments concluded with receipt of the last shipment at WCS on May 1, 2014 [1]. All SWBs were initially stored at WCS above ground in the Container Storage Building (CSB) without temperature control. Upon discovery of the potential of the drums to contain incompatible waste, the SWBs , which were designated to contain Type 3 and/or Type 2 waste, were moved to Modular Concrete Containers (MCCs) in an excavated cell. The void space in the MCCs was filled with pea gravel to a height that provided a two-inch air gap between the gravel and the top of MCC [2]. A thermocouple was attached to the metal pallet between the SWBs to periodically measure the temperature inside the MCC adjacent to the SWBs. Each MCC was then covered with an additional

[1] Type 3 is a drum listed as D001 and contains nitrate salts and sWheat Scoop®. Type 2 is a drum listed as D001 but does not have the same composition as a Type 3 drum. Type 1 is a transuranic (TRU) waste drum that does not contain any prohibited codes.

12-inches of sand. The MCCs and SWBs have remained in this state with plans to remain in the current configuration until the drums can be shipped to WIPP or re-remediated.

Repositioning of the SWBs initiated on May 21, 2014 and completed on May 24, 2014. Section 10.0 contains a graphic of the specific drums, SWBs, and MCCs stored at WCS. Fifty-eight SWBs were placed in 31 small MCCs, and 16 SWBs were placed in 4 large MCCs for a total of 74 SWBs, each containing four 55-gallon drums for a total of 296 drums. Twenty-seven of the small MCCs contain two SWBs stacked vertically, separated by a 4-inch metal pallet, as shown in Figure 1-1. The other four small MCCs contain a single SWB and no metal pallet. In the current study, only the Type 3 drums (113) are addressed – 32 of these drums have the waste inside POCs. The remaining 183 drums are not considered to be reactive.

The Technical Review Team (TRT) was reconvened in this effort to review the previous assessment of the drum's contents [3] and assess controls needed for safe handling, loading, shipping, unloading, and storage in Panel 8 at WIPP. The assessment may include identification of gaps that should be addressed to strengthen the technical basis for transport of the LANL drums stored at WCS and additional controls that may be needed to reduce risk.

One of the challenges identified in the 2020 TRT report [3] was the lack of a definitive initiating reaction that resulted in the breach of Drum 68660 which limited the TRT's ability to assess the potential for another thermal runaway reaction within the 113 WCS RNS drums. For the conclusions in 2022 to be significantly different from those of 2020, new data and/or new tools are required. This report represents the team's efforts to bring new data and new tools to bear on the issue of the WCS drums.

2.0 Technical Review Team Conclusions from July 2020

In July 2020, the Waste Control Specialists Technical Review Team (WCS TRT), commissioned by the Department of Energy (DOE), issued a report of its findings and conclusions based on the data and analytical tools at its disposal [3]. The team examined results from tests completed by LANL, reports on visual inspection and analyses of RNS waste processed at LANL, thermocouple data from waste containers in storage at WCS, technical position papers prepared for DOE's WIPP, recent characterization data completed by Savannah River National Laboratory (SRNL), and other relevant information as needed.

The overarching conclusion of the WCS TRT was that the WCS RNS waste drums had become more stable over time with respect to nitric acid-nitrate salt-sWheat Scoop® reactions, but that existing data were insufficient to eliminate the potential of future reactions leading to thermal runaway of WCS RNS, especially since the initiating reaction could not be determined. At the same time, actions were proposed to reduce the likelihood of a thermal runaway event. Aspects of the team's key judgments are as follows.

Key Judgment 1: The TRT believes that the stability of the WCS RNS waste with respect to autocatalytic thermal runaway due to nitric acid chemistry has and will continue to increase over time as the concentration of nitric acid is depleted from reactions in the drum. However, defining a composition of waste that adequately represents or bounds the chemical and physical properties of the population is a significant technical challenge that the studies to date do not adequately address. Of particular importance, the team concluded that the lack of a definitive initiating reaction that resulted in the breach of Drum 68660 limits the TRT's ability to assess the potential for another thermal runaway reaction within the 113 WCS RNS drums.

Key Judgment 2: Engineering controls can enhance the stability of RNS wastes during interim storage and transportation. Because the WCS drums retain much of their potential chemical energy, insults such as heating, reactive gas build-up, and drying can increase the likelihood of a thermal runaway event. Reduced temperature and continued venting are effective engineering controls to increase the stability of the waste.

The TRT also concluded that the existing drum vents, when functioning as designed, are sufficient to prevent gas build-up and prevent accelerated drying due to excessive head-space ventilation.

3.0 New Information Included in the 2022 Analysis

The conclusions of the TRT are dependent upon the data available for review. For the TRT in 2022 to make key judgments different from those in 2020, the team required either new data and/or new tools with which to evaluate the data. The 2022 team possessed both. This section discusses new information that shaped the conclusions of the team which were not considered previously. Section 4.0 describes an improved calibrated computer model originally developed for the analysis of drum 68660, that enabled the 2022 team to predict the potential for thermal runaway reaction as a function of drum storage conditions and time, evaluate the RNS waste drums considering the full range of storage conditions to which they have been exposed, and consider strategies for safe transport of the RNS waste drums to WIPP. Section 5.0 and Appendix 9.0 describe a more detail analysis of nitric acid oxidation chemistry. The modeling coupled to a detailed understanding of the nitric acid chemistry provides the foundation for the conclusions of this report.

3.1 Behavior of RNS drums before emplacement in MCCs at WCS

The suspect drums, along with the dunnage drums and other TRU waste drums in the SWBs, were shipped from LANL to WCS from April 1, 2014 to May 1, 2014. When the suspect drums arrived at WCS, they were placed into vented SWBs above ground. The SWBs were subsequently placed into MCCs on May 21-24, 2014. The MCCs were initially stored at WCS above ground from May 21 to July 16, 2014 [1]. On June 1, 2014, MCCs were outfitted with thermocouples to monitor temperatures near the drums (Figure 1-1). Figure 3-1 (a) shows modeling results of heat conducted from a drum that experiences thermal runaway to the location of the thermocouple. This calculation assumes the drum ignited and the contents were completely burned, generating an adiabatic flame temperature at the drum, which was assumed to be 900 K. Conduction of this energy to the external soil (assumed to be at 300 K at time zero) and location of the thermocouple was then modeled. Model simulations indicate that a drum experiencing thermal runaway stored at WCS would cool within 40 days. Moreover, the location where thermocouples are placed within an MCC that contains a drum undergoing thermal runaway should experience a temperature change of ~100 K within the first 0 to 10 days after that event. In other words, thermocouples placed within the MCC should be able to detect a thermal runaway event of a drum contained within that MCC.

Figure 3-1 (b) provides the temperature data from a thermocouple attached to the metal pallet for a representative (C-276) MCC and the daily high temperatures at Andrews, TX for that day. Figure 3-1 (c) shows the thermocouple data for C-276 as a function of the daily high temperatures at Andrews, TX, measured on the same day. The temperatures experienced by the MCCs and the surrounding air temperatures are much greater than temperatures in the WIPP repository (300-302 K or 80-84 °F) for that same period [4]. However, both Figure 3-1 (b) and Figure 3-1 (c) indicate temperatures measured within the MCCs are generally slightly elevated above that of the measured daily high air temperatures in the area, suggesting that some level of thermal reactivity from the drums may be contributing to the temperature measured within the MCCs. However, none of the MCC thermocouples recorded temperatures elevated to an extent indicative of a thermal runaway event. Additionally, the measured high temperatures in all MCCs [Figure 3-1 (d)] is decreasing with time, suggesting reactivity of the drums may be decreasing with time.

Since the RNS waste originated from a single heterogenous population, it is assumed that the WCS drums are also reacting in a manner similar to the LANL RNS waste drums. This includes the evolution of gases, including CO_2, CO, N_2O, and H_2. This behavior is consistent with oxidation of organics by nitric acid and/or metal nitrates and radiolysis [5]. Based on what is understood of the temperature dependence of chemical reactions [18], the RNS drums would have been more chemically active during this time above ground due to the increased temperature and thus evolved more gases and consumed a greater amount of nitric acid. The increased reactivity could increase the probability of thermal runaway depending on the balance

between heat generated versus heat dissipated to the environment. However, in the absence of a thermal runaway event, the increased reactivity also would have increased the rate at which the drums were consuming the reactants in the drum [7]. This topic is addressed later in the report.

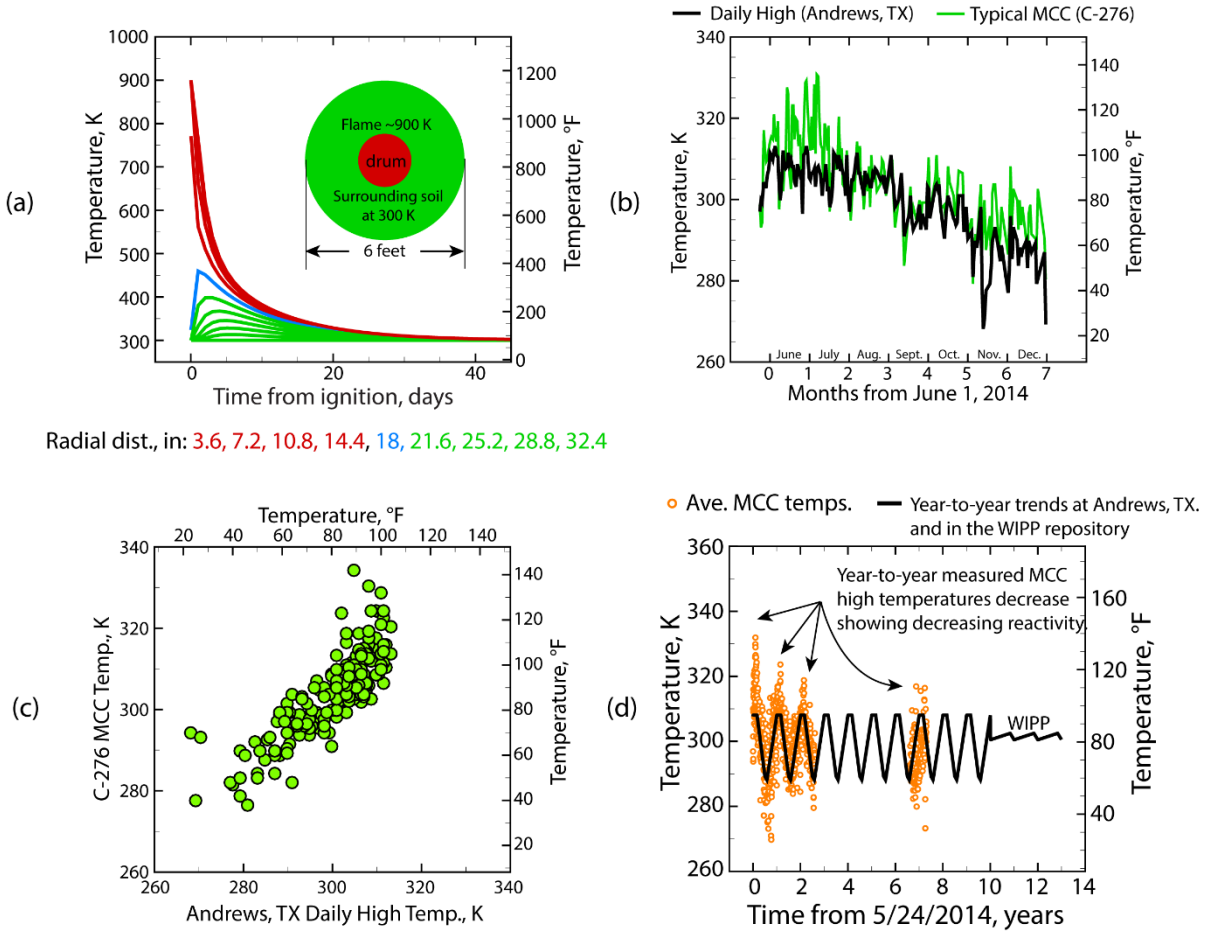

Figure 3-1. (a) Model simulations of heat conducting from a drum experiencing thermal runaway to the surrounding soil 6 feet away. (b) and (c) Comparison of WCS temperature measurements with measurements from a typical MCC (C-276). (d) Year to year measured high temperatures from all MCCs as a function of time. MCCs were stored above ground from approximately May 21, 2014 until July 16, 2014.

3.2 Behavior of similar RNS drums placed in WIPP prior to panel closure

There were 313 RNS drums created at LANL. Of these, 144 drums were placed in Panel 6 and Room 7 of Panel 7 at WIPP (including Drum 68660), 56 were re-remediated at LANL, and 113 are stored at WCS. The first drums, which contained mixtures of metal nitrate salts, nitric acid, and sWheat Scoop®, were prepared at LANL in October 2012 and shipped to WIPP. The last emplacement of RNS into WIPP occurred in February 2014. Following the thermal runaway event with Drum 68660 on February 14, 2014, the closure of Panel 6 and Room 7 of Panel 7 was accelerated through the installation of a chain link barrier, a layer of brattice cloth and 10 feet of mined salt at each entrance. After that, closure of the entrances was completed by erecting a metal bulkhead in the tunnel opening and fitting rubber flashing around the sides to seal off airflow [6]. By late May 2015, Panel 6 and Room 7 of Panel 7 were closed. To our knowledge, no other drum experienced a thermal runaway event other than 68660 during this time.

Apart from Drum 68660, the 143 drums like 68660 were stored for 15 to 30 months at 300-302 K (80-84 °F) [4] without evidence of a thermal excursion leading to an uncontrolled release of contamination into the WIPP repository. Although not conclusive, the thermal excursion in Drum 68660 after only a few days

in WIPP, points to a unique characteristic or unique event for Drum 68660. Significant effort was spent on trying to determine what was unique about the contents of Drum 68660 without resolution [5][7].

3.3 New MCC temperature data from WCS for 2021

Data for the thermocouples measuring the pallet temperature between the SWBs in 34 of the 35 MCCs were available for 2014, 2015, 2016, and 2021 [8]. Data for 2017-2020 were collected by WCS, but they were not requested due to the magnitude of effort required to provide the data sets. The configuration of drums, SWBs, pallet, and the thermocouple in the MCC is provided in Figure 1-1. The metal pallet temperatures in Figure 3-2 are the average of all 34 MCCs. The data for all MCCs, along with the WCS surface temperatures, are plotted in Figure 3-3. The temperature data in Figure 3-3 were smoothed using the Tecplot Focus program [9] using a fixed boundary option.

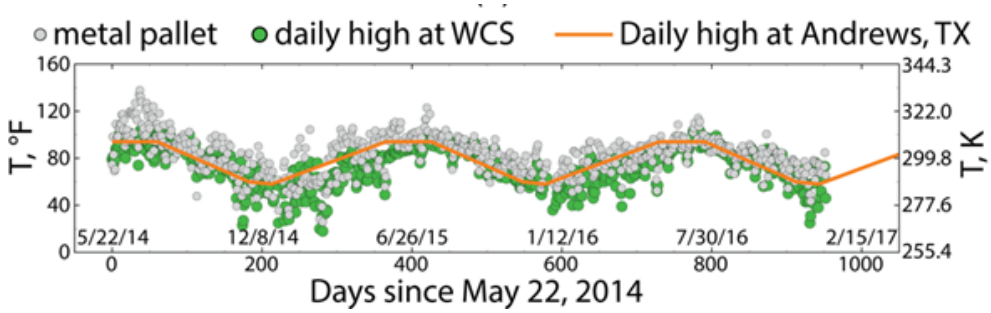

Figure 3-2. Average temperature of all 34 MCCs at WCS.

It should be noted that the data in Figure 3-3 provide a detailed perspective of the thermal conditions of the SWBs within the MCCs. However, because of multiple and varying thermal effects on each MCC, it is not experimentally known how effective the thermocouple is in detecting changes in reaction heat from the drums inside the SWBs. Nonetheless, because each thermocouple is at the same sample location on the pallet under similar thermal conditions year-to-year, the trends of the data in Figure 3-3 deserve consideration. The most significant observation is that there appears to be a trend for the thermocouple temperatures to be cooler year to year. More specifically, the following trends are noteworthy:

1) The thermocouple measurements taken from the metal pallet in the summer are almost always equal to or greater than the surface temperature in 2014, 2015, and 2016. This occurs in 32 of 34 cases. In all 34 MCCs, the 2014 thermocouple summer temperatures exceeded the WCS surface temperatures.
2) Conversely, the thermocouple temperatures from the pallet in the summer of 2021 are less than the surface temperature in 26 of 34 MCCs.
3) There is a general trend [23 of 34 cases] for the temperature to decrease each year. Of the 11 cases which do not exhibit this trend, four of them show only slightly higher temperatures in 2016 than in 2015.

However, while in general the data appear to trend toward cooling, there are some 2021 data which exhibit high temperatures. Most significant are MCCs R21EW and C275 which exhibit temperature maximums in 2021 which are higher than the 2014-2016 data. This suggests that the wastes remain reactive, even after seven years.

In the next section, the Figure 3-3 data will be coupled to a revised computational model originally developed for analysis of Drum 68660 [10] to gain insights into the potential for thermal runaway reactions as a function of storage conditions.

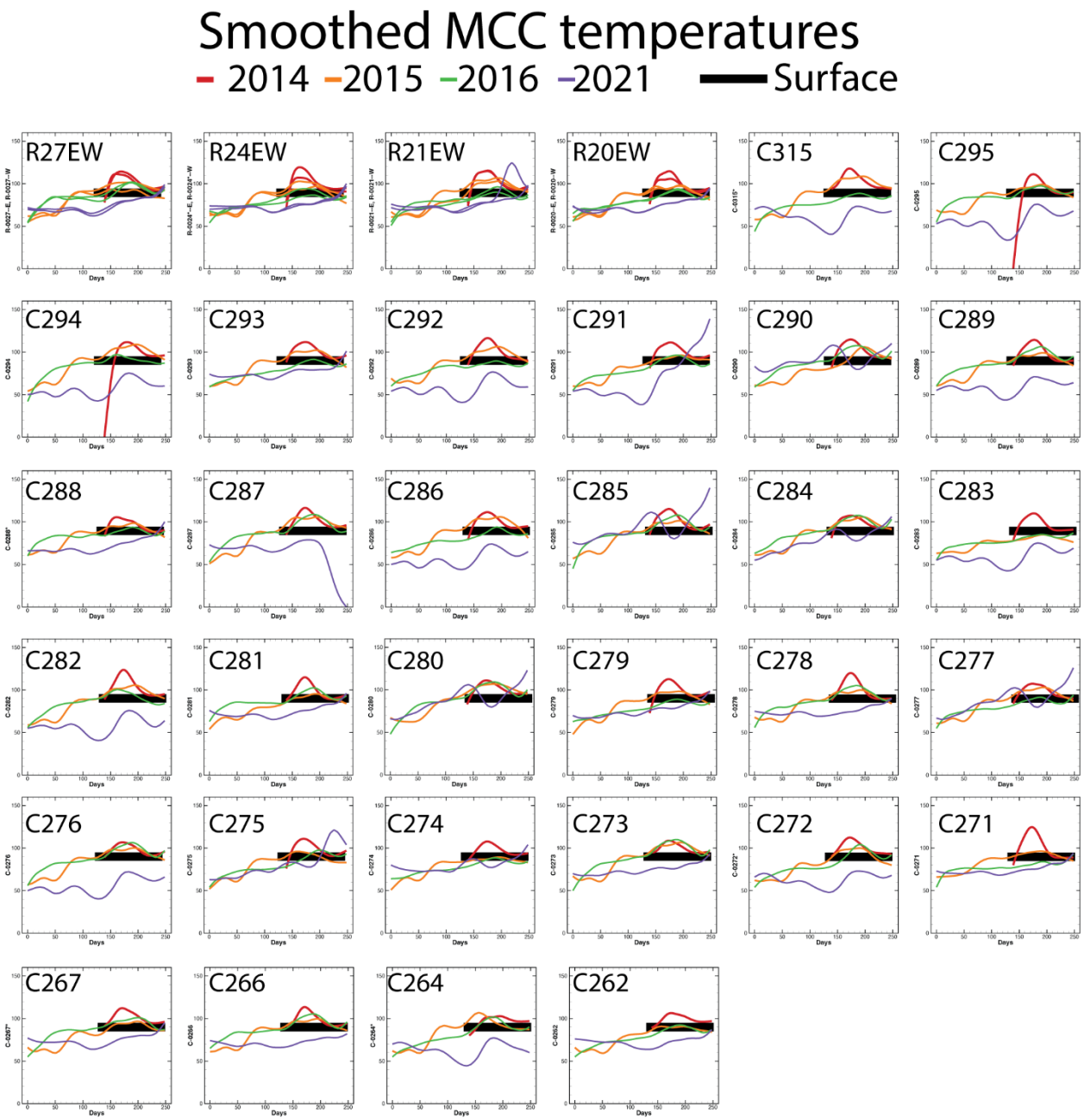

Figure 3-3. MCC metal pallet temperature data from 2014, 2015, 2016, and 2021. Data smoothed using Tecplot Focus. (vertical-axis shows temperature with markings at 0, 50, 100, and 150 °F; horozontal-axis counts days beginning Jan 5). The surface temperature is from May 15 (Day 130) to Sept 12 (Day 250), and the line thickness reflects measurement uncertainty.

4.0 Computer Modeling of RNS Waste Reactivity

A computational model [10] developed originally for analysis of failed Drum 68660 was improved by calibrating with reaction rates with full-scale surrogate drum tests by LANL that were either vented or sealed [11]. The surrogate waste formulation (WB8) [12], which is composed of sWheat Scoop®, neutralized acids, and metal nitrate salts, was designed to be reactive to demonstrate cookoff of RNS waste. This formulation was used to develop the original model, but this formulation may not be representative of long-term aging of the RNS waste. A brief description of the updated RNS waste cookoff model with example calculations for different storage conditions (i.e., time, temperature, and pressure) is given in this section. A more detailed description of the model can be found in Section 8.0.

4.1 Conservation Equations

Thermal runaway reaction (or ignition) of the RNS waste is modeled by solving the conductive energy equation for the vaporization of water (equation 1), decomposition of the RNS waste (equation 2), and radioactivity decay of the waste containing transuranic elements (Table 4-1) [10]. The composition of the RNS waste (W) was defined in the previous TRT report for 68660 [10].

$$H_2O_{(L)} \longrightarrow H_2O_{(g)} \quad \text{(endothermic)} \tag{1}$$

$$C_{2.16}H_{8.64}N_{1.2}O_{7.3}Mg_{0.34}Na_{0.22}Ca_{0.06}Fe_{0.03} \longrightarrow 3.38\ H_2O + 0.45\ CH_4 + 1.2\ CO_2 + 0.6\ N_2 + 0.04\ H_2 + 0.01\ Fe_3O_4 + 0.28\ MgCO_3 + 0.11\ Na_2CO_3 + 0.06\ CaMgC_2O_6 \quad \text{(exothermic)} \tag{2}$$

For a thermal runaway reaction to occur, the heat generated in the chemical and radiolytic reactions must exceed the ability to dissipate the heat [18]. The reaction mechanism considers two reactions (Table 4-1): 1) desorption of moisture "M" (equation 5) and 2) decomposition of the RNS waste "W" (equation 6). Pressure, from evolution of gaseous products, is determined using a gas equation of state with an analytical expression for deformation of spherical defects caused by internal gas generation balanced by material strength in both gas permeable and impermeable waste. This model approach is robust and has been used for a wide range of materials from the older explosives [13] to newer explosives [14].

Reaction rates can be considered "constant", "deceleratory", or "acceleratory" as discussed by Erikson [17]. These terms refer to how the reaction proceeds with respect to decomposition. We have investigated all three reaction types and have concluded that the deceleratory mechanisms mimic the observed gas evolution and other data best [36]. Provided the waste is vented (n = 0 in Eq. 6 of Table 4-1), the rates will continue to decelerate in time until the reactive waste concentration goes to zero. However, if gas exchange through the vent is significantly restricted (n=5.4 in Eq. 6 of Table 4-1), the rates will accelerate with decomposition potentially leading to a thermal runaway reaction and breaching containment.

Table 4-1. RNS waste thermal ignition model with nomenclature and parameters found in the Section 8.0; "M" refers to Moisture, "W" to Waste, "G" to Gas, and "S" to Solid. The full nomenclature listing is in Table 8-1.

Energy	$\rho C_p \frac{\partial T}{\partial t} = \nabla \cdot (k \nabla T) + h_{r1} r_1 + h_{r1} r_2 + \dot{q}_{decay}$	(3)
Mechanism	$\mathrm{M} \xrightarrow{1} \mathrm{M}_g;\ \mathrm{W} \xrightarrow{2} 5.67\ \mathrm{G} + 0.46\ \mathrm{S}$	(4)
Reaction 1 rate	$r_1 = A_1 \exp\left(\frac{-E_1 + \zeta_1 \sigma_1}{RT}\right)[\mathrm{M}]$	(5)
Reaction 2 rate	$r_2 = A_2 \left(\frac{P}{P_o}\right)^n exp(-E_2/RT)[W]$	(6)
Microsoft Excel function NORMINV	$\xi_1 = \mathrm{norminv}([M]/[M]_o)$	(7)
Pressure	$P = z\rho RT/M_w$	(8)

LANL ran four 55-gallon drum tests in which each drum contained WB8 and was about 65% full of stratified surrogate waste [15]. Two (A, B) of the four (A, B, C, D) 55-gallon LANL drum tests [11] were used to calibrate the reaction model. Drum Test A was vented at room temperature, while Test B was sealed. Drums C and D were slowly heated to 333 K (140 °F) at 0.6 K/h. The initial plan was to have Drum C vented and Drum D sealed, but gas exchange through Drum C became restricted, and it behaved like Drum D. [11]

As part of the model development [Figure 4-1(a) and (b)], drum Tests A and B were used to determine E_2/R (17360 K) and n (5.4) for reaction 2 (equation 6 of Table 4-1). Parameters for reaction 1 (equation 5 of Table 4-1) were taken from the literature [12]. The pressure exponent, n, was set to zero for the vented predictions in Figure 4-1(a). The large pressure exponent makes the surrogate waste extremely pressure sensitive. In fact, even a few psig can cause the reaction rates to increase significantly. For example, an increase of 8 psi can cause the reaction rates to increase by over an order of magnitude, e.g.,

$[(14.7+8)/14.7]^{5.4} = 10.4$. Drum tests C and D, which were heated at 0.6 K/h to 333 K, were used to partially validate the thermal runaway model described in Table 4-1.

It is important to note that the manner in which Drum C plugged was not representative of the plugging mechanism that may have occurred in the case of Drum 68660. As part of the configuration for Drum Test C, a cap and sampling system were installed over the drum vent (Figure 4-2, left). This created backpressure in the drum higher than the backpressure with the drum vent alone. It also restricted the venting cross-sectional area. The backpressure caused the reactions in the drum to accelerate, and the reduced venting area limited the release of gas. This enabled the drum to begin to experience autocatalytic reactions tending toward thermal runaway. The reactions and heat in the drum caused the drum vent to become further restricted. When the temperature and pressure reached 388 K (239 °F) and ~14 psig, an audible "pop" was heard, and a visible disturbance of the top insulation near the vent port was observed. This was followed by copious release of vapors. Immediately after the popping noise, the drum vented over the next ten minutes to ambient pressure, and the reaction was successfully quenched even though the drum temperature had reached 388 K (239 °F). The popping noise has been attributed to the dislodging of the carbon frit in the drum vent (Figure 4-2, right).

Predictions in Figure 4-1(b-d) were made assuming the waste was either impermeable or permeable to gas as defined in [15][16]. The primary difference between permeable and impermeable waste is that the gases in permeable waste can permeate throughout the bed and fill any available headspace gas. Gases generated in impermeable beds remain in isolated defects. Thus, the impermeable model option predicts shorter times for thermal runaway in sealed systems since the pressures are higher than in permeable drums where decomposition gases can fill headspace within the drums.

The appendix provides additional validation of the model using surrogate data from several small-scale experiments performed at both Sandia National Laboratory (Sandia Instrumented Thermal Ignition (SITI) experiment) and Pacific Northwest National Laboratory (accelerating rate calorimeter [ARC] experiments) [38][39].

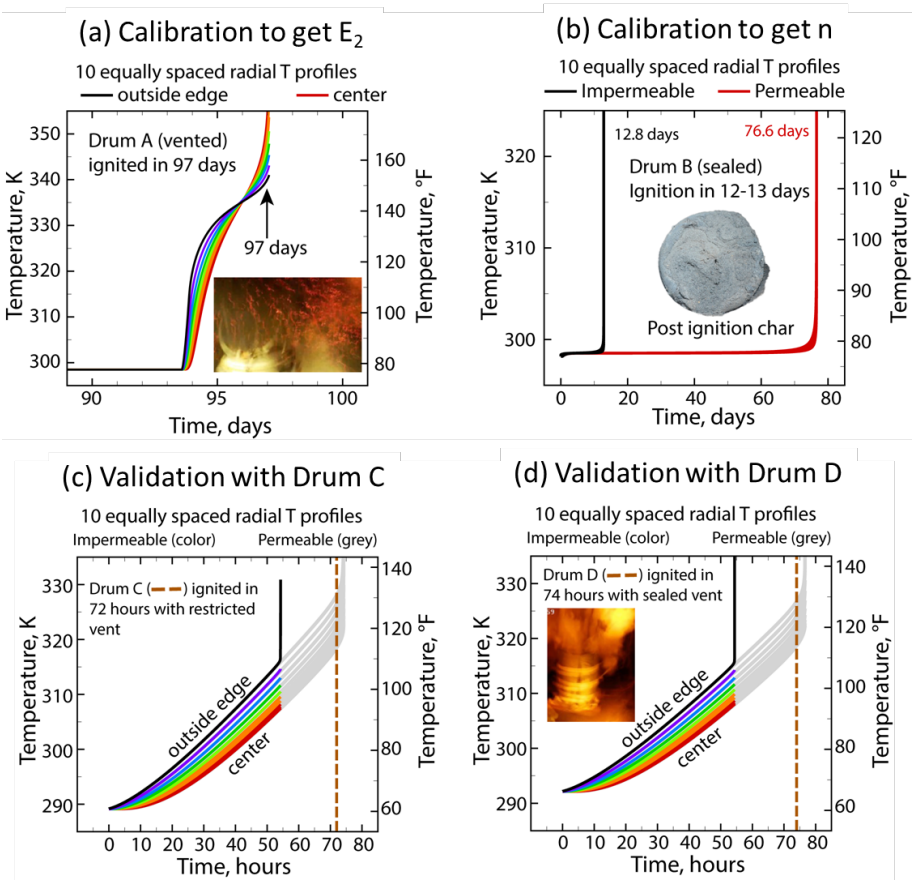

Figure 4-1. Predicted temperatures for drums (a) A, (b) B, (c) C, and (d) D as a function of time and radial thermocouple position (different colored lines). Drums A and B were used for calibration of the model and Drums C and D were used for validation. The drum boundary temperatures are shown as dashed gray lines. The solid color and gray lines represent the predicted radial temperatures within the drums. Inset photos in (a) and (d) were taken at LANL just after thermal ignition.

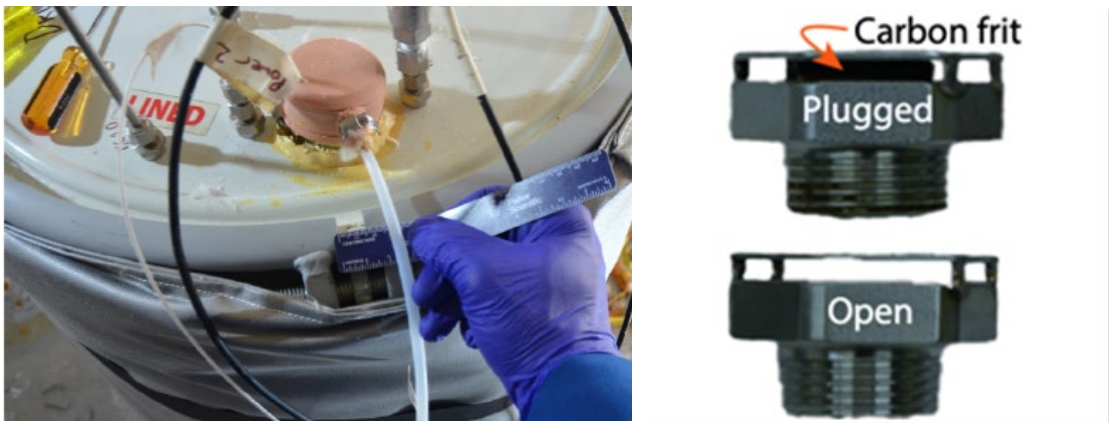

Figure 4-2. Gas sampling configuration for LANL Drum Test C (left). Images of plugged and open drum vents (right).

4.2 Drum 68660 Thermal Runaway at WIPP

A final validation of the model was made by predicting the time at which Drum 68660 experienced a thermal runaway reaction in the WIPP repository on February 14, 2014. One challenge with making the Drum 68660 prediction is prescribing the appropriate boundary condition for the drum and knowing when the drum may have sealed. Prior to shipping, the outside drum temperature for Drum 68660 is assumed to be 272 K (30 °F) which was the average of temperatures at Los Alamos, NM during January 2014. The

drum was stored at LANL in an unheated building until being shipped to WIPP on January 29, 2014. In the simulations, we assume the drum was placed in the repository at a measured temperature of ~300 K (80 °F [4]) , which was warmer than the surface temperature 272 K (30 °F).

Table 4-2 explores potential times during handling and transport when gas exchange through the Drum 68660 vent could have become restricted. The time of the plugging event is taken as time zero in Table 4-2 and the thermal runaway time is defined as February 14, 2014. Thus, the model predicts Drum 68660 could have had a runaway reaction between 36 and 62 days with the actual ignition occurring after 42 days as shown in Table 4-2 if 1) the Drum 68660 vent became restricted and caused the reaction rates to accelerate and 2) if the restricting event occurred during movement of the drum after the final gas analysis. The lowest error (-15%) between the model predictions and observed ignition time for 68660 corresponds with Drum 68660 plugging after the gas analysis on January 3, 2014. A major finding of this study is that the model predicts the time for thermal runaway of Drum 68660 accurately if we assume the drum vent was plugged. These results suggest the contents of drum 68660 may not have been fundamentally different from the overall RNS waste stream.

Table 4-2. Ignition of Drum 68660 assuming drum was inadvertently sealed during movement using a pressure dependent deceleratory model in Section 8.0.[a]

Potential vent restriction event:	Gas analysis[b]	Loaded on truck	Shipped to WIPP	Placed in repository
Time zero	1/3/2014	1/28/2014	1/29/2014	1/31/2014
Thermal runaway time	2/14/2014	2/14/2014	2/14/2014	2/14/2014
Days to thermal runaway, days	42	17	16	14
Predicted ignition for an impermeable bed, days (% error)	35.6 (-15%)	10.8 (-36%)	9.8 (-39%)	7.8 (-44%)
Predicted ignition for a permeable bed, days (% error)	62.3 (+48%)	37.5 (+121%)	36.5 (+128%)	34.5 (+146%)

[a]Predictions in this table are based on the pressure-dependent model described in Section 3 with the surface temperature at 272 K (30 °F) and a repository temperature at 300 K (80 °F). The version of this model, that assumed the decomposition products were adequately vented with no restrictions, did not predict any ignition, even after 13 years.
[b]Most likely scenario based on model predictions.

Figure 4-3(a) and (b) show predicted internal temperatures and pressures within Drum 68660, respectively. These predictions were made by assuming the drum plugged after the gas analysis on January 3, 2014. Because gas samples are withdrawn with a septum and not from the drum vent, there remains a possibility that the drum vent was already plugged at the time of gas analysis, but that scenario is not considered here. Two predictions are presented in Figure 4-3(a) and (b) by assuming the waste bed was either permeable or impermeable to the decomposition gases. The predicted ignition times ranged from 39 to 63 days with the actual ignition occurring after 44 days as shown in Table 4-2. Although, the temperature graphs in Figure 4-2 (a) have been truncated for clarity, the pressure graphs in Figure 4-3(b) have not been truncated. At thermal ignition, the predicted pressures using the impermeable and permeable bed assumptions are 0.7 MPa (102 psig) and 0.3 MPa (44 psig), respectively. These high pressures would cause breach of the drum as failure was shown to occur at 0.17 MPa (24 psig) in the original WIPP TRT report [10].

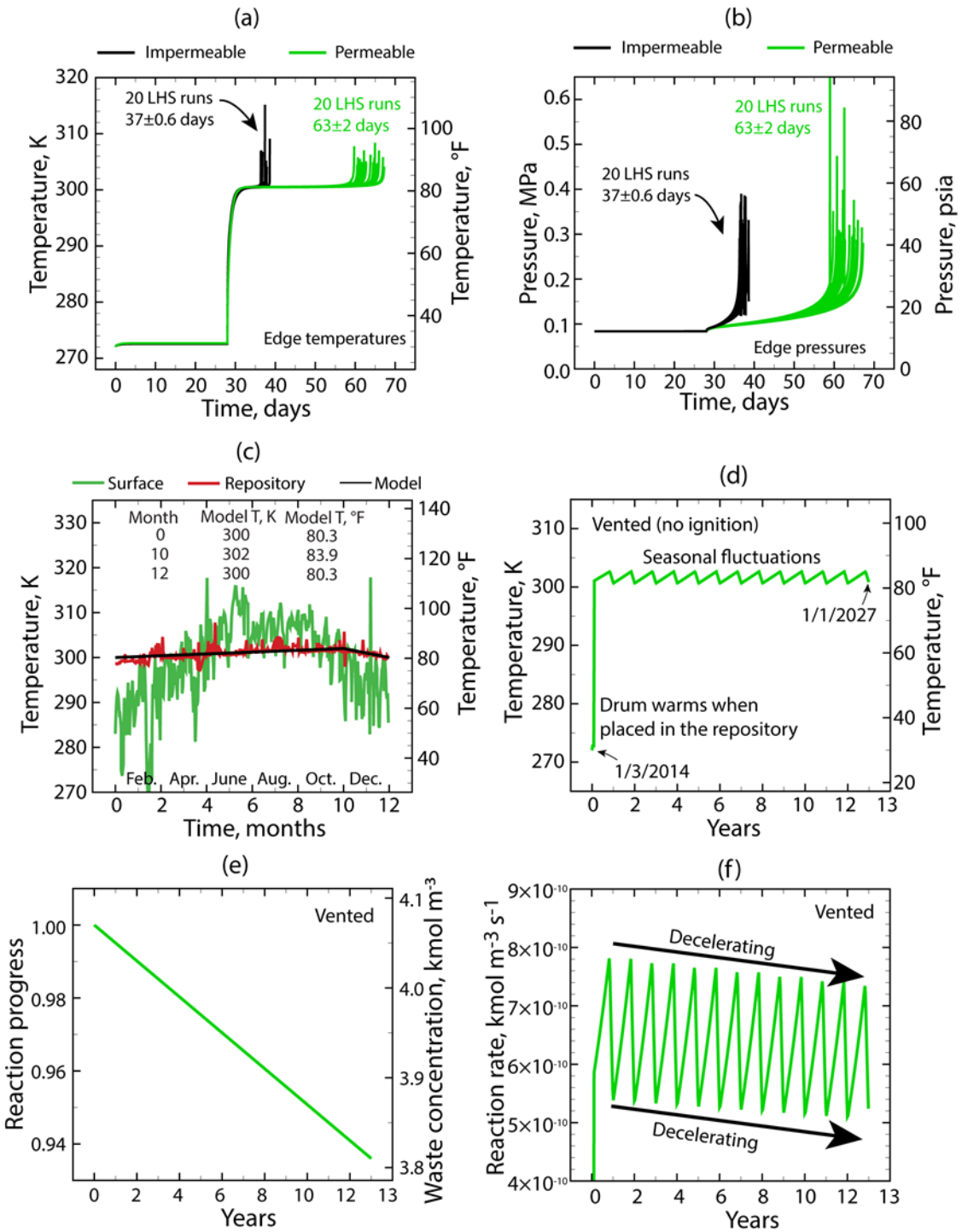

Figure 4-3. Predicted (a) radial temperatures and (b) pressure for sealed Drum 68660 with impermeable and permeable waste. (c) Surface temperatures and repository temperatures at WIPP. (d) Predicted radial temperatures for vented Drum 68660 for 13 years. No ignition is predicted in (d). Predicted (e) reaction progress and waste concentration and (f) reaction rate from vented prediction in (d). Note: LHS = Latin hypercube sampling.

For the predictions in Figure 4-3(a) and (b), the temperature in the repository was assumed to be constant at 300 K (80 °F). However, realistic repository temperatures fluctuate due to seasonal temperature changes as unconditioned surface air is used for repository ventilation [see Figure 4-3(c)]. Furthermore, the repository temperatures are different than the surface temperatures due to the large thermal mass of the

repository. Both the surface temperatures and repository temperatures shown in Figure 4-3(c) were measured in 2021 and represent the boundary fluctuations in the repository for 13 years as shown in Figure 4-3(d) [4]. The mildly fluctuating reservoir temperature (± 2 K or 4 °F) was used for subsequent simulations of the WCS drums.

Drum 68660 was simulated with the boundary temperature shown in Figure 4-3(d) with the pressure exponent (*n)* set to zero to mimic a vented drum. The model predicts that Drum 68660 would not have had a thermal runaway reaction, even after 13 years, if the drum was not allowed to pressurize (i.e., the vent remained open). Therefore, Drum 68660 and its contents are like those of the other RNS drums stored in the WIPP repository and at WCS. Figure 4-3(e) shows the predicted progress of the reaction of an RNS drum over the 13-year simulation time going from 1.00 on January 1, 2014 to 0.936 on January 1, 2027 with a corresponding drop in the waste concentration from 4.07 kmol m^{-3} to 3.81 kmol m^{-3}. Similarly, the rate of reaction 2 is shown in Figure 4-3(f) which shows decreasing reactivity of the waste if the drum is vented. Decreasing reactivity with time is consistent with decreasing gas concentations reported by Funk for the LANL RNS waste drums [18].

Consequently, the technical basis for positing that Drum 68660 experienced a runaway reaction because gas flow through the drum vent became restricted leading to pressurization of the drum rather than unique chemistry is significant. This is based on the following points.

- Extensive population analyses of the RNS waste drums at LANL (56) and WCS (113) concluded that the drums were not statistically different in composition, and process history. Therefore, because the drums were filled from a common waste stream population, they could be studied as one heterogeneous population, and findings from one member of the population could be used to predict the behavior of the other [7].
- Nitric acid is the principal oxidant in this reaction system at lower temperatures (<60 °C). Although Drum 68660 contained approximately 2 gal of neutralized nitric acid, 28 other drums in the WCS population (25%) had more neutralized nitric acid than Drum 68660 [7].
- The sister drum (Drum 68685) to Drum 68660 showed no unique chemical components when processed [10].
- Real-time radiography of Drum 68660 and other drums in the WCS population, taken after the drums were filled, revealed no unique characteristics of Drum 68660.
- The nominal drum temperature of Drum 68660 was 272 K (30 °F) from when the lid was sealed (December 4, 2013) until the date it was placed into WIPP (January 31, 2014). The nominal drum temperature was 300 K (80 °F) from when the drum was placed into WIPP until ignition (February 14, 2014). The model does not predict ignition for a vented RNS drum population below 327 K (130 °F).
- The model accurately predicts the behavior of Drum 68660 if the vent is plugged. It also correctly predicts the behavior of other large- and small-scale tests containing nitric acid, metal nitrate salts, and sWheat Scoop®.

The difference between Drum 68660 and other drums at WIPP and WCS could be related to restriction of gas flow through the drum vents in 68660 leading to a pressure build up and acceleration of the reactions (see discussion of nitric acid chemistry in Section 5.0).

4.3 Model Application to WCS Drums

Following the thermal runaway event with Drum 68660, 113 other RNS waste drums containing similar plutonium-processing waste were shipped May 21-24, 2014, in SWBs from LANL to WCS. The SWBs were subsequently placed into MCCs. The MCCs were initially stored at WCS in the CSB above ground

from May 21, 2014 to July 16, 2014 [1]. The CSB did not contain temperature control. After the period of above-ground storage, the MCCs were placed below grade and covered with sand (see Figure 1-1(a-c)).

In the current modeling work, the daily high temperatures measured at Andrews, TX were taken to be representative of the RNS drums within the MCC while stored at WCS, since the daily temperature measured in the MCCs were nearly the same as these daily high temperatures (see Figure 3-2). The yearly fluctuations as shown in Figure 4-4(a) were assumed to be similar from year to year. The model assumes the drums contents are an impermeable bed; although, some predictions assume the bed is permeable to show the sensitivity of this model assumption. The impermeable bed assumption is conservative. The model was used to predict the behavior of the drums under various conditions and time scales.

The solid orange lines in Figure 3-2 and Figure 4-4(a) represent the assumed boundary temperature of the WCS drums based on the measured high temperature in Andrews, TX [19]. Figure 4-4(b) shows the boundary temperatures for the MCCs over a 10-year period at WCS (t=0 when the SWBs were placed in the MCCs), followed by placement in WIPP, in year 10, where they are held for three years where the repository temperature is assumed to follow the yearly modulation discussed previously with Figure 4-3(c). The orange dashed lines in Figure 4-4(a) represent a ±4 K (±7 °F) uncertainty in the MCCs boundary. Thermal runaway was not predicted for any of the boundary conditions that varied between 288 K – 308 K ± 4 K) as long as the drums remained vented and the drum's pressure did not increase.

The temperature of the RNS drums in the MCCs initially exceeded the daily high temperatures when they first arrived at WCS since the MCCs were exposed to direct sunlight as shown by the measured MCC temperatures [small gray circles in Figure 4-4(a)]. Figure 4-4(c) shows a vented simulation where the initial temperature was increased to 328 K within the first 25 days, and then cooled as the MCC was buried. The model did not predict a thermal runaway reaction when the external drum temperature reached 328 K after 25 days. Rather a temperature excursion, i.e., self-heating due to chemical reactions, was predicted in which the temperature increased to 335 K (143 °F) followed by cooling rather than thermal runaway. Similar temperature excursions were found in studies of RNS waste simulants [5]. If the temperature had been higher than 328 K (131 °F) for an extended period (55 days), then ignition would have been predicted. As specified in the annotation in Figure 4-4(c), a vented MCC with temperatures of 329 K (132 °F), 330 K (134 °F), and 332 K (137 °F) could have ignited as they sat in the sun for ~55 days prior to burial. However, the calculations were conservative and did not include the night and day fluctuations in temperature.

Figure 4-4(d) presents predicted radial temperatures for the WCS drums assuming that the drums were sealed after being placed underground at an initial temperature of 308 K (94 °F) at WCS. Predicted ignition times for both impermeable and permeable waste beds were 2 days and 11 days, respectively. The predictions in Figure 4-4(d) were made from the time that the drums arrived at WCS in early 2014. Figure 4-5(a) presents predicted radial temperature profiles for drums that were vented for 10 years and then put into the WIPP repository (at 80 °F) wherein the drums were sealed. After 10 years of decomposition, the waste density changes from 785 kg m^{-3} to 736 kg m^{-3} as the nitric acid and reactive waste are consumed. Predicted ignition times for both impermeable and permeable waste beds were 10 days and 60 days after the initially vented drum is placed into the repository and accidentally sealed, respectively. These plots highlight the importance of keeping the RNS drums vented and ensuring gas exchange after emplacement at WIPP.

One possible way to arrest a thermal runaway reaction in a plugged drum is to lower the drum temperature. If the drum becomes plugged and is simultaneously cooled, the ignition times increase as shown in Figure 4-5(b). For example, by lowering the temperature to 279 K (43 °F), the model with an impermeable bed does not predict thermal ignition for at least three years. Similarly, by lowering the temperature to 287 K (57 °F), the model with a permeable bed does not predict thermal ignition for at least three years.

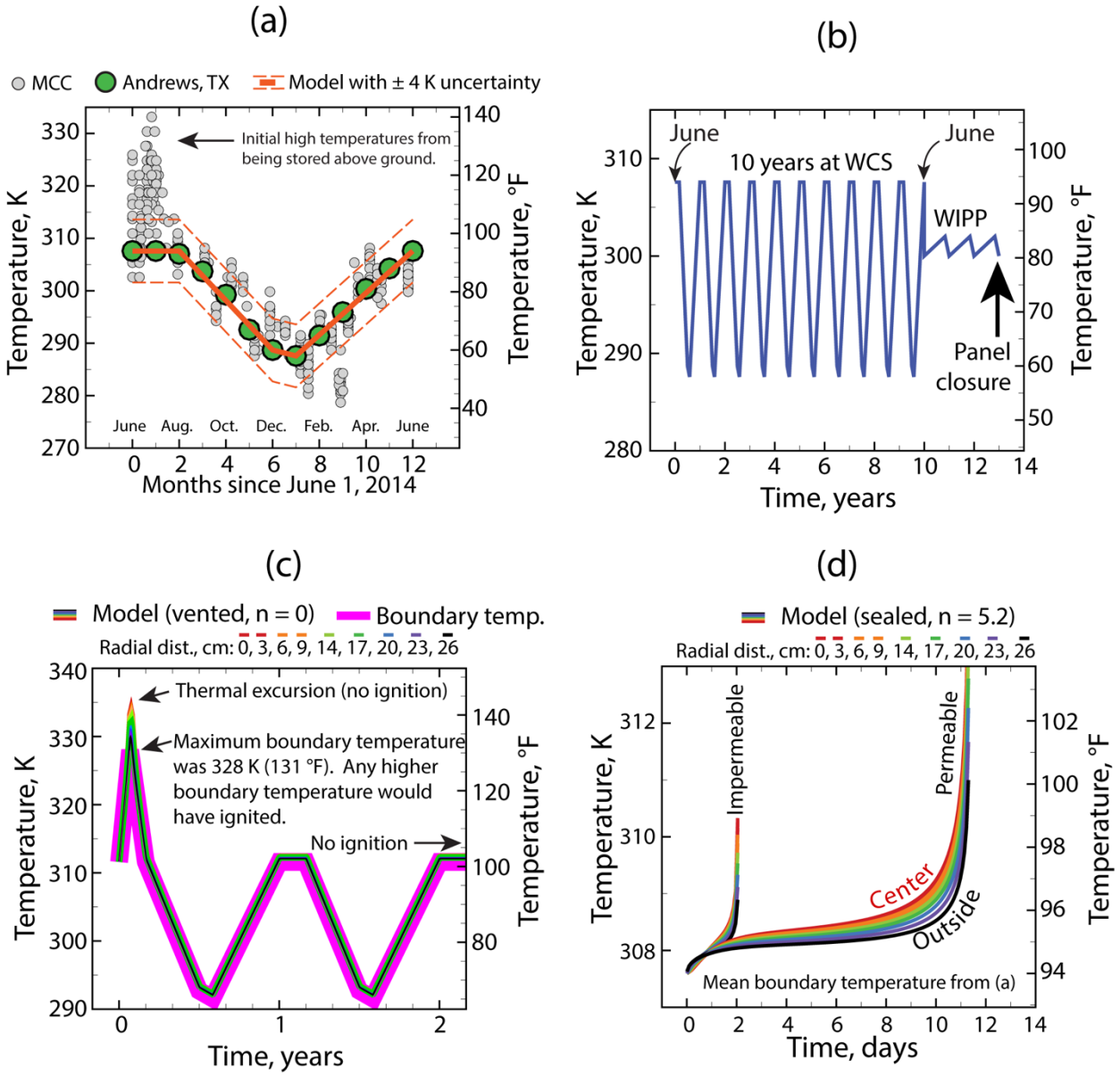

Figure 4-4. Boundary temperatures for modeling of WCS drums for (a) 1 year and (b) 13 years. The green circles in (a) are average monthly high temperatures from [19]. The gray circles in (a) are MCC measured temperatures. The solid orange line in (a) is the model boundary temperature which is repeated in (b) for 10 years followed by the temperatures of the WIPP repository from Figure 4-3(c). (c) Vented drum predicted temperatures with the initial drum temperature increased to 328 K within the first 25 days, and then cooled as the MCC was buried. (d) Sealed drum predictions assuming the bed is either permeable or impermeable.

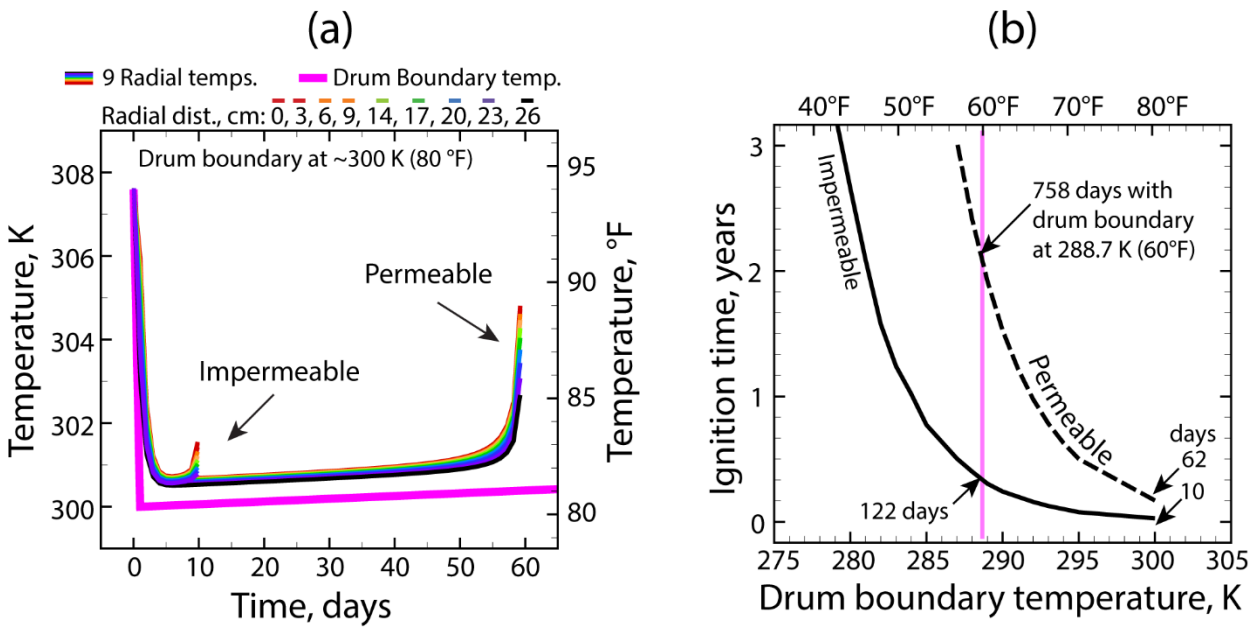

Figure 4-5. Simulations showing ignition when a vented WCS drum is placed in repository and then becomes inadvertently sealed. The boundary temperature in (a) uses the expected repository temperature from Figure 4-4(c). The boundary temperature in (b) assumes the drums are cooled after being plugged.

4.4 Model Summary

A simple pressure-dependent deceleratory model has been calibrated with surrogate waste and validated with both large-scale and small-scale data collected at LANL, Sandia National Laboratory (SNL), and Pacific Northwest National Laboratory (PNNL) using surrogate waste (see Section 8.0). In some of these validations, the impermeable bed calculations were closest to the experimental measurements. In others, the permeable bed calculations matched the experimental data best. These observations indicate that the model bounds the behavior of the waste with contents that are undoubtedly heterogeneous with different types of job control waste. Consequently, the similarity of the reactive salts outweighs the diverse nature of the individual drums.

The model adequately predicted the thermal runaway of Drum 68660 assuming the drum vent was plugged, allowing it to pressurize. Model results indicate that if Drum 68660 had not been plugged, then ignition would not have occurred. The ignition of Drum 68660 during the cooler months supports the conclusion that the drum became plugged, as the model also predicts that cooler temperatures would extend the time to ignition. Funk gives some possible mechanisms leading to plugging of drum 68660: 1) low carbon filter permeability that is insufficient for high gas flow rates, 2) internal polyvinylchloride (PVC) bag may have sealed against the outlet, 3) bags of magnesium oxide may have been piled on top of the drum and covered/sealed the filter outlet, and 4) condensed reaction products may have clogged the carbon filter [15].

Nonetheless, since there were no eyewitnesses to the thermal ignition event involving Drum 68660, it is unclear if and how the vent became plugged. The only bases supporting the hypothesis that the Drum 68660 vent became plugged leading to pressurization of the drum is the model described above, the experimental observations that sealed drums of surrogate waste experienced thermal runaway, and the known nitric acid oxidation chemistry (see Section 5.0).

Simulations indicate that vented drums are not prone to thermal runaway below 328 K (131 °F). However, sealed drums can thermally runaway at WIPP temperatures (80-84 °F) due to the pressure sensitivity of the waste even after sitting for years. Simulations of the WCS drums at 308 K (94 °F) indicate that ignition may occur in sealed drums after 2 to 11 days, depending on whether the waste was permeable or

impermeable. The pressure sensitivity decreases with age as the moisture, nitric acid, and reactive waste is depleted. After 10 years of venting, a plugged drum could thermally runaway between 10 to 60 days at 300 K (80°F), implying a fivefold increase in the time to achieve ignition due to aging. By dropping the plugged drum temperature to 279-287 K (43-57 °F), depending on the bed permeability assumption, its ignition could be delayed for at least three years. However, this requires the drums to be maintained at these lower temperatures for all three years.

5.0 Nitric Acid Reactions and Drum 68660

5.1 Autocatalytic Nitric Acid Oxidation Reactions

The products found in the debris expelled from Drum 68660 in Panel 7 Room 7 in WIPP were consistent with an exothermic oxidation reaction between sWheat Scoop®, metal nitrate salts, and nitric acid [3][10]. These reactions produced gaseous products that led to the breach of Drum 68660. As previously discussed [10], the LANL RNS waste at WCS arose from the nitric acid processing of plutonium that contained a mixture of metal nitrate salts with entrained nitric acid, neutralized liquids, and sWheat Scoop®, a wheat-based absorbent composed of starch (65-70% by mass) and proteins/enzymes (14% by mass). The final composition of the metal nitrate salts, and the acidity of the residual liquid, was dependent on whether the process feed originated from ion-exchange, in which the salts were washed with 3.3 M HNO_3 to remove residual plutonium, or oxalate precipitation, in which the salts were washed with water to reduce acid catalyzed decomposition of oxalic acid [5].

Although metal nitrate salts can thermally decompose in the absence of organics to generate HNO_3, NO_2, and O_2, the temperatures required for these reactions typically exceed 573 K (572 °F) [10]. Organics lower the degradation temperature for metal nitrate salts [5][20][21]. In automatic pressure tracking adiabatic calorimeter experiments on surrogate waste, mixtures of metal nitrate salts and sWheat Scoop®, were found to self-heat at temperatures as low as 333 K (140 °F), but mixtures could not be found to initiate the reactions at room temperature without the addition of nitric acid [5][10]. Thus, attention turned to oxidation reactions involving nitric acid which are known to lead to thermal runaway reactions [22].

After reviewing the complex nitrogen redox cycle involved in the solution phase oxidation of alcohols and carbohydrates, Duval proposed that nitric acid reactions with the RNS waste contents could lead to exothermic reactions [22]. When coupled with the positive feedback loop from reduced gaseous nitrogen oxide species, Duval concluded that nitric acid "can initiate autocatalytic thermal runaway reactions and explosive gas generation" [22][23]. The autocatalytic nature of these reactions is highly dependent on the concentration of nitric acid, the concentration of organic substrate, and temperature (as discussed below).
In the RNS drums, the sWheat Scoop® is in excess (fuel rich), and the nitric acid is the limiting reagent. As the nitric acid is depleted through reaction with sWheat Scoop®, the acidity of the waste should decrease with time. This is supported by the pH measured for the moistened solids from the six LANL RNS drums that were reprocessed which had pH ranging from 2.7-5.2. That pH level is too high to support autocatalytic nitric acid oxidations chemistry [3]. Thus, the stability of the WCS RNS waste with respect to autocatalytic thermal runaway due to nitric acid chemistry should increase over time as the nitric acid is depleted from reactions in the drum (Key Judgment 2).

5.2 Oxidation of Carbohydrates by Nitric Acid

This section discusses nitric acid chemistry and nitric acid oxidation of the key functional groups in carbohydrates and their oxidation products, i.e., alcohols, aldehydes, and carboxylic acids. The origin of the autocatalytic reaction is discussed and how the interconversion of nitrogen oxide species is key to sustaining the oxidation reactions. A more-detailed discussion of these reactions is contained in Section 9.0.

Many (but not all) nitric acid oxidation reactions are autocatalytic in which there is an induction period followed by an exothermic reaction with rapid product evolution and heat generation. In some cases, these oxidation reactions have led to runaway reactions and explosions [24]. The mechanisms for oxidation reactions by nitric acid are complex. In general, nitric acid rarely oxidizes organic compounds directly, but instead forms reduced nitrogen oxide species, such as NO_2 and HNO_2, which react with the organic compounds [25].

In the liquid and gas phase, nitric acid can slowly undergo thermal decomposition at room temperature to nitrogen dioxide (reaction 9). In the liquid phase, nitrogen dioxide reacts back with water to form nitric acid (reaction 10, 1 x 10^8 $M^{-1}s^{-1}$) based on its solubility in water, 7 x 10^{-3} M at^{-1} at 295 K (i.e., Henry's law coefficient, which is the partial pressure of NO_2 in the air vs concentration in water) [26]. In the gas phase, nitrogen dioxide is in fast equilibrium with nitric oxide (reaction 11).

$$4HNO_3 \rightleftharpoons 4NO_2 + 2H_2O + O_2 \quad (9)$$

$$3NO_2(g) + H_2O\ (l) \rightarrow 2HNO_3\ (l) + NO\ (g) \quad (10)$$

$$2NO_2 \rightleftharpoons 2NO + O_2\ (\text{gas phase}) \quad (11)$$

In the RNS drums, the nitric acid can react with the sWheat Scoop®, which is primarily composed of starch, a branched polysaccharide composed of α–glucose units. The most reactive functional group in starch is the alcohol unit (-OH). When nitric acid concentrations are >1M, the autocatalytic oxidation of alcohols, aldehydes, ketones, and carboxylic acids has an induction period followed by an exothermic reaction with rapid product evolution and heat generation [27]. It has been determined that nitrous acid (HNO_2) is the key reagent in the autocatalytic reaction [25][27][28].

Although the concentration of nitrous acid is low in nitric acid [29], it has been shown that seemingly insignificant concentrations of nitrous acid, 10^{-7} to 10^{-4} M, influence the induction period of the oxidation reaction [27]. Moreover, the induction time can be shortened by the addition of nitrite ions (NO_2^-) or nitrous acid (HNO_2) or lengthened by the addition of nitrite scavengers [27][30].

The nitric acid oxidation of alcohols is autocatalytic because two moles of nitrous acid are produced for every mole consumed (reaction 12, where R is an aliphatic or aromatic hydrocarbon), which leads to additional exothermic oxidation reactions and thermal runaway [25][27][31].

$$RCH_2OH + HNO_2 + HNO_3 \rightleftharpoons RCHO + 2HNO_2 + H_2O \quad (12)$$

In the LANL RNS drums, the temperature dependent evolution of CO_2 and N_2O is consistent with nitric acid oxidation of organics in a fuel rich environment. With the limited solubilities of the nitrogen oxides, the gaseous nitrogen oxide species need to be kept from escaping the drum to support the feedback mechanism leading to an autocatalytic exothermic reaction. Venting prevents volatile reactive species from building up and continuing to react while providing a route for dissipating excess heat through evaporation of water and volatile species, as demonstrated in drum-scale testing [11]. For more mechanistic details of the nitric acid oxidation of alcohols, see Appendix, (Section 9.0).

It is anticipated that the LANL RNS waste drums at WCS have been undergoing slow oxidation reactions and radiolysis over the last eight years, which produce gaseous products [3]. For the LANL RNS waste, the estimated level of reactivity implied from the rate of CO_2 and N_2O generation from the SWB and drums indicates that it would take decades to consume all the organics in the drums. Moreover, for all the RNS drums stored at LANL until re-remediated in 2018, the concentration of these gases had decreased with time, indicating a decrease in reactivity and lower heat generation. Thus, the stability of the WCS RNS

waste with respect to autocatalytic thermal runaway due to nitric acid chemistry should increase over time as the nitric acid is depleted from reactions in the drum.

5.3 Summary of Nitric Acid Oxidation Chemistry

Based on the discussion above and the modeling studies, it is proposed that nitric acid oxidation of sWheat Scoop® in a sealed (non-vented) drum is likely responsible for the autocatalytic thermal runway reaction in Drum 68660. The mechanisms for oxidation reactions by nitric acid are complex and the reactivity depends on many factors including concentration of the nitric acid, substrate, and any other additives, such as acids, nitrite ions, or metal ions, as well as temperature and pressure. Nitric acid forms reduced nitrogen oxide species, such as NO_2, N_2O_4, HNO_2, NO^+, and NO, which can exothermically oxidize organic compounds and produce additional reactive species, such as HNO_2, to continue the reaction. Many of these nitrogen species are gases, with limited solubility, that react in solution to form a positive feedback loop that leads to an autocatalytic thermal runway reaction. Thermal runaway can be initiated by relatively small increases in partial pressures of the NOx compounds.

Under the proposed mechanisms, autocatalytic reactions are possible at high acidities (>1-2M HNO_3) under fuel lean conditions and not under fuel rich environments, such as those found in the LANL drums (see Section 9.0). It is proposed that nitric acid is the limiting reagent in the oxidation reactions and the concentration of nitric acid is decreasing over time due to reaction with sWheat Scoop®, and other organics, such as oxalic acid and triethanolamine, if present. As with the 56 drums of LANL RNS waste, it is proposed that the 113 Type 3 drums at WCS are undergoing slow oxidation reactions which is consuming the nitric acid and sWheat Scoop® generating CO_2 and N_2O (in addition to other gases from radiolysis). Thus, the stability of the WCS RNS waste with respect to autocatalytic thermal runaway due to nitric acid chemistry should increase over time as the nitric acid is depleted from reactions in the drum. However, it is important to note that while the reactivity of the wastes at WCS should have decreased over the past eight years, the majority of the reactive components within the wastes remain.

6.0 Expanded Key Judgments for 2022

6.1 Modeling of Drum 68660 and the WCS Drums

A model of the WCS waste drums is described in Sections 4.0 and 8.0 to evaluate the potential for thermal runaway reactions during transport and final disposition of the drums in the WIPP salt repository. Modeling the WCS drums is challenging since the heterogeneous contents of the drums are similar but not the same, and they cannot be examined due to the nature of the radioactive waste. Even with such difficulties, a model of Drum 68660 failure was revised and parameterized by several small-scale and full-scale surrogate waste experiments to allow for prediction of thermal runaway reactions. Once parameterized, the model was able to replicate the thermal runaway event of Drum 68660 and other test data evaluating reactions between nitric acid, nitrate salts, and sWheat Scoop®. Different models were evaluated in which the reaction rates were “constant”, “deceleratory”, or “acceleratory. It was concluded that the deceleratory mechanisms represent the observed data best.

Based on model observations, two major factors increase the reactivity of the waste: 1) an increase in temperature of the waste due to an increase in the ambient temperature; and 2) increase in internal pressure due to the restricted gas exchange through the drum vents due to flow restrictions at the waste bag, drum, POC, or SWB interfaces. Blocking of interstitial pores leading to an impermeable bed scenario as a direct result of transportation activities is deemed improbable [18].

The model indicates that increased pressure played a significant role leading to thermal runaway of Drum 68660. This is also consistent with the nitric acid oxidation chemistry which requires the gaseous nitrogen oxide species to participate in the reactions that could lead to an autocatalytic thermal runaway reaction.

Consequently, the model predicts that vented WCS drums will not thermally runaway unless the external temperatures are unusually high (328 K or 130 °F). No predicted signs of ignition were observed for the vented WCS drums after ten years of storage at WCS and 3 years of storage within the WIPP repository where the drums will eventually be entombed in the WIPP repository.

6.2 Nitric Acid Reactions and Aging of the Waste

The contents of the drums of LANL RNS waste from nitric acid processing of plutonium originated from a single heterogenous population in which the mass fractions of common components can vary between drums [12]. The evolution of CO_2, CO, N_2O, and H_2 from the 56 LANL RNS barrels is consistent with oxidation of organics by nitric acid and/or metal nitrates and radiolysis. The concentrations of these gases, measured from the headspace of the SWB overpack, were found to be temperature dependent – increasing and decreasing with increasing and decreasing external temperature. Additionally, the concentrations of CO_2, CO and N_2O were found to decrease over time, indicating a decrease in the rate of chemical reaction. LANL modeled the gas generation rates for a vented drum assuming a single reaction with an Arrhenius temperature dependence [36]. Very good fits were obtained to the measured gas concentrations from Drum 68685 (sibling to Drum 68660 that breached at WIPP), and the model predicted a reduction in gas generation by a factor of 1.6 by cooling the waste from 300 K (80 °F) to 290 K (62 °F) and a factor of 24 for cooling from 300 K (80 °F) to 278 K (40 °F).

The 113 drums at WCS are also expected to be undergoing temperature-dependent chemical reactions that are slowly consuming the nitric acid, nitrate salts, and sWheat Scoop® while generating gases and other products. The model calculates that 6% of the reactive waste will be consumed over the first 12 years of RNS drum life. Therefore, although storage of the waste at WCS has decreased its reactivity, there is sufficient potential chemical energy to fuel a thermal runaway reaction under certain conditions.

The effect of short-term (21 weeks) aging on the thermal stability of RNS surrogates was studied by LANL [18]. Funk reported that the self-heating onset temperature increased as a function of time which led to a reduction in the rate of chemical reaction with time [18]. However, there are no long term (years) studies on the effects of aging on the stability and/or reactivity of RNS waste.

6.3 Pressure Effect and Runaway Reactions

A predictive model describing autocatalytic reactions with sWheat Scoop® and nitric acid was calibrated against full-scale experiments and validated against small-scale experiments and Drum 68660. Model calculations indicate that increases in pressure have an immense effect on the reaction rates. This model has a 5.4 exponent dependence on pressure changes which predicts that a pressure increase of 8 psi above atmospheric pressure will translate into an order of magnitude increase in reaction rates. An increase of 20 psi elevates reaction rates by a factor of 100. It is estimated that the drum lid would fail at 30±3 psi [15]. In other words, wastes at WCS are still capable of thermal runaway if conditions arise that lead to an increase in pressure in the POC, waste drum, or SWB boundaries. The pressure could increase in the drums because of failure of the vent, restriction in the vent due to external conditions (e.g., bags of MgO placed on top of the drum) or internal conditions (e.g., a bag inside the drum covering the vent), reactions leading to a gas impermeable waste, or other conditions.

Modeling studies are consistent with the hypothesis that Drum 68660 experienced conditions that led to a pressure increase during transport or emplacement in WIPP. While not statistically significant, the probability of one of the drums at WCS experiencing a catastrophic pressure increase during handling at WCS, transport to WIPP, and handling and emplacement at WIPP is roughly 1 in ~250, based upon the single Drum 68660 event and assuming none of the other drums emplaced at WIPP (143 drums) or currently located at WCS (113 drums) have experienced thermal runaway.

With the waste drums inside SWBs, it is impossible to determine whether the drum vents have become compromised without inspecting or changing them. However, even ensuring that the WCS drum vents are not restricted at WCS is not sufficient assurance against pressurization, because it is assumed that flow through the Drum 68660 vent was not restricted when it left LANL. Thus, the probability of an event that restricts gas flow through the vents during the transfer of wastes from WCS to their final disposition at WIPP cannot be estimated with any reasonable degree of technical certainty.

The computer model predictions highlight the importance of pressure in leading to a thermal runaway reaction within these systems and indicates that pressure should **not** be allowed to increase in the drums, POC, or SWBs. This necessitates a mitigation strategy that ensures the drums remain vented during handling, transport, storage, and emplacement. Not knowing the specific actions and/or conditions that led to Drum 68660 pressurization is a significant problem for a path forward for the WCS drums. As previously discussed, there are a range of potential pathways leading to drum pressurization, and any mitigation strategies must consider all feasible internal and external events that could lead to the pressurization of the drums. For example, initiating pressurization events include, but are not limited to, 1) carbon filter vents with low permeability that is insufficient for high gas flow rates, 2) internal polyvinyl chloride (PVC) bag or other solid contents that may seal against the outlet vent, 3) bags of magnesium oxide or items that may be placed on top of the drum and obstruct the filter vent outlet, and 4) condensed reaction products that may clog the carbon filter of the drum vent.

6.4 Temperature Effects at Repository Conditions

Modeling describes the chemical instability of the WCS drums at or near the storage conditions at either WCS or the WIPP repository. Exothermic chemical reactions within the drums and insulation provided by the surroundings lead to both gas generation and heating of the drums. According to the model, drums that are stored in the WIPP repository at or near the expected repository temperature profile will experience some reaction between nitric acid, metal nitrate salts, and organic materials and gas generation, but the reactions will expend themselves over time before thermal runaway can occur, if vented.

For a vented system, the model predicts that a thermal runaway is only possible when the external temperature exceeds 328 K (130 °F) for an extended time [see Figure 4-4(c)]. This is because the model is deceleratory with respect to gas concentrations, and the model shows that the rates do not accelerate due to thermal dissipation if the external boundary temperature does not exceed 328 K (130 °F).

For a sealed system, modeling indicates that cooling can be used to counteract the pressure effect on the reaction rate by a corresponding drop in the temperature of the waste drum throughout handling at WCS, transport to WIPP, and handling and emplacement at WIPP. Figure 4-5(b) shows no ignition for an impermeable bed (worst case scenario) when the temperatures are maintained at 279 K (43 °F). Similarly, Funk [18] identified a target cooling temperature of 278 K (40 °F) for the transport of RNS drums back to LANL for re-remediation. This amount of cooling would counteract the deleterious effects of an event that lead to an increase in pressure in a system with restricted gas flow through the vent, up to the failure pressure of a drum lid. Above this temperature the probability of thermal runaway increases. Much below this temperature, water begins to freeze and, therefore, may have unpredicted consequences since this has not been investigated.

If the drums were moved during the winter months, the reduced temperature would decrease the reactivity of the wastes during transport. However, this temperature mitigation strategy alone would not be significant enough of a temperature adjustment to counteract the potential effect that vent plugging has on the reactivity of the wastes when emplaced at WIPP (see Section 4.3).

6.5 Summary

For the TRT in 2022 to make key judgments that would differ significantly from those in 2020, the team required either new data and/or new tools with which to evaluate the data. As such, the team brought together some limited new data on the temperature history of the drums at WCS, refined a model originally developed for analysis of RNS waste reactivity and drum 68660, and reevaulated the reaction mechanisms for the autocatalytic nitric acid oxidation of carbohydrates to determine if different conclusions could be reached for the disposition of the WCS drums.

The revised calibrated model provides deeper insights into the roles of pressure, temperature, and extent of reaction on waste stability after 8 years. The revised calibrated model shows that pressurization of the drum could have led to the thermal runway reaction in drum 68660 in 2014, which supports the hypothesis that the contents of the drum were not fundamentally different from the overall remediated nitrate salt (RNS) waste stream. It also offers a predictive tool to evaluate the possibility of thermal runaway reaction in subsequent years. Pressure and temperature continue to represent the two most important characteristics of the WCS drums to manage during transportation, storage, and emplacement of the WCS drums at WIPP.

Because the waste drums retain most of their reactive components, i.e., metal nitrate salts and sWheat Scoop®, even after eight years, the risk of a thermal runaway reaction has not been eliminated. Mitigating strategies could be developed to address both temperature and pressure. However, not knowing the cause of Drum 68660 pressurization prevents decision makers from tailoring mitigating strategies based on the initiating event. Consequently, mitigating strategies must address all the feasible internal and external events that could lead to drum pressurization.

7.0 References

1. Brandt, M. T., Maggiore, P., *Written Concurrence for Correction of Waste Manifests for Waste Shipped to Waste Control Specialists Facility*, ERID-260197, Los Alamos National Laboratory, Los Alamos, NM, August 14, 2014.
2. Lee, S. Y., *Thermal Evaluations for Mixed Organic and Nitrate Salt Drums in Interim Storage at the WCS Federal Waste Facility.* SRNL-STI-2018-00095, Savannah River National Laboratory, February 2018.
3. WCS TRT, Waste Control Specialists Technical Review Team Report, SRNL-RP-2020-00146, Aiken, 2020.
4. Hobbs, M. L., data received from Mark Pearcy by way of Kerry Watson of the DOE Carlsbad Field Office on May 3, 2022.
5. Clark, D. L., Funk, D. J. Chemical Reactivity and Recommended Remediation Strategy for Los Alamos Remediated Nitrate Salts (RNL) Waste. LA-UR-15-22393; Los Alamos National Laboratory, Los Alamos, New Mexico, 2015.
6. DOE 2014, Waste Isolation Pilot Plant Nitrate Salt Bearing Waste Container Isolation Plan, Carlsbad, New Mexico: U.S. Department of Energy Carlsbad Field Office.
7. Wilmarth, W., Fink, S., Looney, B., Pizzino, A., Washington, A., Young, J. Stability Study of LANL RNS Waste at Waste Control Specialists; SRNL-RP-2018-00644; Savannah River National Laboratory: Aiken, SC, 2018.
8. Hobbs, M. L., data received from Ryan Williams of Waste Control Specialists; permission to use data provided by D. Nickless of DOE-EM on April 6, 2022.
9. Tecplot Focus User's Manual, Tecplot Focus 2021 Release 2, https://tecplot.azureedge.net/products/focus/current/focus_users_manual.pdf (accessed 18 May 2022).
10. Wilson, D. L., Baker, M. L., Hart, B. R., Marra, J. E., Schwantes, J. M., Shoemaker, P. E., Knotek, M., Michalske, T. A., and Klaus, D., Waste Isolation Pilot Plant Technical Assessment Team Report, Savannah River National Laboratory, SRNL-RP-2014-01198, Aiken, 2015.
11. G. R. J. Parker, G. R. J.,Holmes, M. D., Heatwole, E. M., Leonard, P., and Leibman, C. P., Drum-scale Testing of the Thermolytic Response of a Remediated Nitrate Salts (RNS) Surrogate Waste Mixture, Los Alamos National Laboratory Report LA-CP-16-20038, Los Alamos, 2016.
12. Weisbrod, K. R., Veirs, D. K., Funk, D. J., Clark, D. L., Salt Composition Derived from Veazey Composition by Thermodynamic Modeling and Predicted Composition of Drum Contents, LA-UR-16-21651, March 11, 2016.
13. Hobbs, M. L., Kaneshige, M. J., Cookoff of Black Powder and Smokeless Powder, *Propellants, Explosives, Pyrotechnics,* **2021**, 484-493, 2021.
14. Hobbs, M. L., Kaneshige, M. J., Coronel, S., "Vented and sealed cookoff of powdered and pressed e-CL-20," *Journal of Energetic Materials, **2021**,* 39 (4), 1-20.
15. Funk, D. J., The Path to Nitrate Salt Disposition, LA-UR-16-21760, February 22, 2016.
16. Hobbs, M. L., Brown, J. A., Kaneshige, M. J., and Aviles-Ramos, C., A Micromechanics Pressurization Model for Cookoff, *Propellants, Explosives, Pyrotechnics, **2022,*** e202100155.
17. Erikson, W. W., Application of various global decomposition model forms to energetic material cookoff, in *13th International Detonation Symposium*, Norfolk, 2006.
18. Funk, D., Use of Lower Temperatures to Provide Protection for Remediated Nitrate Salt (RNS) During Handling and Transportation to WCRRF-Revision 1, Los Alamos National Laboratory memorandum to Derik Gordon, EM2016-5229 R1, Los Alamos, 2016.
19. US Climate Data--Andrews Texas, 2022. [Online]. Available: https://www.usclimatedata.com. [Accessed February 2022].

20. Smith, H. D.; Jones, E. O.; Schmidt, A. J.; Zacher, A. H.; Brown, M. D.; Elmore, M. R. Gano, S. R. Denitration of High Nitrate Salts Using Reductants. PNNL-12144, Pacific Northwest National Laboratory: Richland, Washington, 1999.
21. Wu, K.-T.; Zavarin, E. Thermal Analysis of Mixtures of Nitrates and Lignocellulosics Materials. *Thermochim. Acta,* **1986**, *107*, 131-148.
22. Duval, P. B. Safety Evaluation of Nitric Acid Reactions with Polysaccharides. LA-UR-18-27835; Los Alamos National Laboratory: Los Alamos, New Mexico, 2019.
23. Duval, P. B.; Chancellor, C. J. Safety Evaluation of Remediated Nitrate Salt Waste. LA-UR-19-23350; Los Alamos National Laboratory: Los Alamos, New Mexico, 2019.
24. Usachev, V. N.; Markov, G.S. Incidents Caused by Red Oil Phenomena at Semi-Scale and Industrial Radiochemical Units. *Radiochem.,* **2003**, *45*, 1-8.
25. Ando, M.; Fujita, M.; Izato, Y.-i.; Miyake, A. Autocatalytic Reaction Mechanism of Nitric Acid and Formic Acid Mixtures Based on Thermal and in situ Raman Spectroscopy Analysis. *J. Therm. Anal. Calorim.* **2020**, *144*, 553-562.
26. Lee, Y.-N.; Schwartz, S. E. Reaction Kinetics of Nitrogen Dioxide with Liquid Water at Low Partial Pressure. *J. Phys. Chem.,* **1981,** *85*, 840-848.
27. Bazsa, G.; Epstein, I. R. Kinetics and Mechanism of Autocatalytic Nitric Acid Oxidations. *Comments Inorg. Chem.,* **1986***, 5*, 57-87.
28. Horváth, M.; Lengyel, I.; Bazsa, G. Kinetics and Mechanisms of Autocatalytic Oxidation of Formaldehyde by Nitric Acid. *Int. J. Chem. Kinet.,* **1988**, *20*, 687-697.
29. Ziouane, Y., Leturcq, G., New Modeling of Nitric Acid Dissociation of Acidity and Temperature. *ACS Omega,* **2018**, *3*, 6566-6576.
30. Van Woezik, B. A. A., Westerterp, K. R., The Nitric Acid Oxidation of 2-octanol. A Model Reaction for Multiple Heterogeneous Liquid-Liquid Reactions. *Chem. Eng. Process.,* **2000**, *39*, 521-537.
31. Ross, D. S., Gu, C.-L., Hum, G. P., Malhotra, R., Oxidation of Benzyl Alcohols by Nitrous and Nitric Acid in Strong Sulfuric Acid Media. *Int. J. Chem. Kinet.* **1986**, *18*, 1277-1288.
32. Wieczorek-Ciurowa, K.; Kozak, A. J., The Thermal Decomposition of $Fe(NO_3)_3 \bullet 9H_2O$. *J. Therm. Anal. Calorim.,* **1999**, *58*, 647-651.
33. Keely, W. M., Maynor, H. W., Thermal Studies of Nickel, Cobalt, Iron, and Copper Oxides and Nitrates. *J. Chem. Eng. Data,* **1963**, *8*, 297-300.
34. Melnikov, P., Nascimento, V. A., Arkhangelsky, I. V., Zanoni Consolo, L. Z., Thermal Decomposition Mechanism of Aluminum Nitrate Octahydrate and Characterization of Intermediate Products by the Technique of Computerized Modeling. *J. Therm. Anal. Calorim.,* **2013**, *111*, 543-548.
35. MacDougall, C. S.; Bayne, C. K.; Roberson, R. B. Studies on the reaction of Nitric Acid and Sugar. *Nucl. Technol.,* **1982**, *82*, 47-52.
36. Robinson, B. A.; Leibman, C. P. Interpretation of Headspace Gas Observations in Remediated Nitrate Salt Waste Containers Stored at Los Alamos National Laboratory. LA-UR-22661, 2015.
37. Prout, E. G., Tompkins, F. C., The Thermal Decomposition of Potassium Permanganate, *Transactions of the Faraday Society, **1944***, 40, 488-498.
38. Scheele, R. D., McNamara, B. K., Schwantes, J. M., Hobbs, D. T., Minette, M. J., Barrett, C. A., Thermoanalytical investigatoin of the reactions causing the transuranic waste drum breach that occurred in the Waste Isolation Pilot Plant, *Thermochimica Acta, **2017**,* 76-87.
39. Scheele, R. D., Minette, M. J., McNamare, B. K., Schwantes, J. M., Thermochemical Reactivity Hazards of TRU Waste Constituents--16075, *Waste Management Conference*, Phoenix, 2016.

40. McKay, M. D., Beckman, R. J., and Conover, W. J., A Comparison of three methods for selecting values of input variables in the analysis of output from a computer code, *Technometrics,* **1979**, 21, 239-245.
41. Rogers, J. L., Nicewander, W. A., Thirteen Ways to Look at the Correlation Coefficient, *The American Statistician,* **1988**, 42 (1), 59-66.
42. Castellan, A., Bart, J. C. J., Cavallaro, S., Nitric Acid Reaction of Cyclohexanol to Adipic Acid. *Catalysis Today* **1991**, *9*, 255-283.
43. Kumar, V., Yang, T., HNO_3/H_3PO_4-$NANO_2$ Mediated Oxidation of Cellulose – Preparation Characteristics of Bioabsorable Oxidized Cellulose in High Yields and with Different Levels of Oxidation. *Carbohyd. Polym.* **2002**, *48*, 403-412.
44. Albright, L. F., Carr, R. V. C., Schmitt, R. J., Nitration: An Overview of Recent Developments and Processes In *Nitration*; Albright, L. F.; Carr, R. V. C.; Schmitt, R. J., Eds; ACS Symposium Series 623; American Chemical Society: Washington, DC, 1996; pp 1-9.
45. Zacharia, I. C., Deen, W. M., Diffusivity and Solubility of Nitric Oxide in Water and Saline. *Ann. Biomed. Eng.* **2005**, *33*, 214-22.
46. Kay, W. B., The Physicochemical Properties of Pure Nitric Acid. *Chem Rev* **1960**, *60*, 185-204.
47. Ogata, Y., Sawaki, Y., Kinetics of the Nitric Acid Oxidation of Benzyl Ethers to Benzaldehyde. *J. Am. Chem. Soc.* **1966**, *88*, 5832-5837.
48. Ogata, Y., Sawaki, Y., Matsunaga, F., Tezuka, H., Kinetics of the Nitric Acid Oxidation of Benzyl Alcohols to Benzaldehydes. *Tetrahedron* **1966**, *22*, 2655-2664.
49. Aellig, C., Neuenschwander, U., Hermans, I., Acid-Catalyzed Decomposition of the Benzyl Nitrate Intermediate in HNO_3-Mediated Aerobic Oxidation of Benzyl Alcohol. *ChemCatChem.* **2012***, 4*, 525-529.
50. Longstaff, J. V. L., Singer, K., The Kinetics of Oxidation by Nitrous Acid and Nitric Acid, Part II. Oxidation of Formic Acid in Aqueous Nitric Acid. *J. Chem. Soc.* **1954**, 2610.
51. Svetlakov, N. V., Nikitin, V. G., Nikolaeva, A. E., Oxidation with Nitric Acid of Aliphatic Alcohols and Diols to Carboxylic Acids. *Russ. J. Org. Chem.* **2007**, *43,* 773-774.
52. Mason, C., Brown, T. L., Buchanan, D., Maher, C. J., Morris, D., Taylor, R. J., The Decomposition of Oxalic Acid in Nitric Acid. *J. Sol. Chem.* **2016**, *45*, 325-333.
53. Singh, V., Ali, S. Z., Acid Degradation of Starch. The Effect of Acid and Starch Type. *Carbohydr. Polym.* **2000**, *41*, 191-195.
54. Smith, T. N., Hash, K., Davey, C.-L., Mills, H., Williams, H., Kiely, D. E., Modifications in the Nitric Acid Oxidation of D-Glucose. *Carbohydr. Res.* **2012,** *350*, 6-13.
55. Coppinger, E. A., Pilot Plant Denitration of Purex Waste with Sugar. Hanford Atomic Products Operation, Richland, Washington; HW-77080, 1963.

8.0 Appendix. Detailed Description of the Model

8.1 Model and Parameters

Details of the RNS waste thermal ignition model are provided in this Appendix. The model describes exothermic decomposition of RNS waste composed of moisture, organic cat litter, neutralized acids, and nitrate salts into equilibrium products as discussed in [10].[2]

$H_2O_{(L)} \longrightarrow H_2O_{(g)}$ + 44 J kmol^{-1} (endothermic) or M$\longrightarrow H_2O_{(g)}$ [A.1]

$C_{2.16}H_{8.64}N_{1.2}O_{7.3}Mg_{0.34}Na_{0.22}Ca_{0.06}Fe_{0.03} \longrightarrow$ [A.2]
3.38 H_2O + 0.45 CH_4 + 1.2 CO_2 + 0.6 N_2 + 0.04 H_2 + 0.01 Fe_3O_4 + 0.28 $MgCO_3$ + 0.11 Na_2CO_3 + 0.06 $CaMgC_2O_6$ - 528 J kmol^{-1} (exothermic)

or W$\longrightarrow$ 5.67 G + 0.46 S

Energy generated by decomposition is usually dissipated via thermal conduction. However, when the energy is generated faster than can be dissipated, thermal runaway (i.e., ignition) occurs as temperature-dependent reaction rates accelerate uncontrollably. Following thermal ignition, the reactive waste is consumed in post-ignition burn, high pressures cause confinement failure, and pressure relief may cause release of radioactive waste. Post-ignition burn and plume dissipation are beyond the scope of the current report.

Ignition can be determined by solution of the conductive energy equation from Table 4-1, which includes the reaction rates for reactions [A.1] and [A.2]. Literature values were used for the water desorption rate, r_1, and reaction parameters (A_1, E_1, σ_1) [13]. Several reaction rate forms were considered for the waste decomposition and included a constant zero-order rate, $r = Aexp(E/RT)$; a deceleratory 1st order simple Arrhenius rate, $r = Aexp(-E/RT)[W]$; an acceleratory distributed activation energy rate, $r = Aexp([E + \xi\sigma]/RT)[W]$; and a Prout-Thomkin [37] acceleratory rate, $r = Aexp(E/RT)\alpha^n[1-(1-10^{-p})\alpha]^m$. Of these different rate models, the only form that matched Funk's [18] observed deceleration due to aging was the deceleratory 1st order simple Arrhenius rate. However, this simple reaction form was not consistent with LANL's drum data [11] that shows significant acceleration of the reactions caused by confinement which resulted in rapid pressurization of the drums. To accommodate both observations (rate deceleration in vented drums and rate acceleration in sealed drums) we modified the simple first order Arrhenius rate expression by using a pressure multiplier:

$$r_2 = A_2\left(\frac{P}{P_o}\right)^n exp(-E_2/RT)[W]. \quad [A.3]$$

The only parameters required for this simple rate expression are the pressure exponent, n, and the activation energy E_2. Pressure is calculated with the ideal gas equation-of-state for both permeable and impermeable beds as discussed in detail in [16]. Pressure in impermeable waste is higher than in permeable waste since the gases are retained within the local pores rather than percolating through the bed and commingling with the headspace gases. More details regarding the pressurization model can be found in [16].

[2] These reactions were determined from the best estimate of the waste composition in drum 68660 which was composed of the metal nitrate hydrates, organic cat litter (sWheat Scoop®), and neutralized acids as discussed further in Reference [10]. The product hierarchy was determined by doing an equilibrium calculation at 400 K and 1 atm. The simplification is obtained by adding the stoichiometric coefficients for the gases, which sum to 5.67, and the stoichiometric coefficients for the solids, which sum to 0.46. The average molecular weight of the decomposition gases (G) and the solid species (S) can be obtained by doing simple molar averages. The heat of formation for G and S were obtained using Hess's law.

Table 8-1 presents the parameters used in the waste decomposition model. An underlying assumption of the model is that all the RNS drums are filled with the same population of waste, and the contents are sufficiently described in the available documentation Most of these parameters are discussed in [10]. However, the parameters for the waste decomposition rate are different, and the pressurization model includes parameters for the micromechanics pressurization model.

Table 8-1. Nomenclature and model parameters

Symbols	Description	Value	Units
$\ln(A_1)$, $\ln(A_2)$	Natural logarithm of the pre-exponential factors	35, 35	$\ln(s^{-1})$
C_p	Specific heat with linear interpolation and constant extrapolation	1150 (273 K) 1570 (343 K)	J kg^{-1} K^{-1}
E_1/R, E_2/R	Activation energy over *R*	25000, 17360	K
σ_1/R	Standard deviation of activation energy over R	2500	K
[G]	Gas concentration from waste decomposition	Initially 0	$kmol/m^3$
M, W, G, S	Refer to Moisture, Waste, Gas, and Solid	n/a	n/a
h_{fi} (i = M, M_g, W, G, S)	Heat for formation for i^{th} species	$-285.8\acute{}10^6$, $-241.8\acute{}10^6$, $-1377\acute{}10^6$, $-233\acute{}10^6$, $-1265\acute{}10^6$	J/kmol
h_{ri} (i = 1, 2)	Heat of reaction for i^{th} reaction (Hess's law)	$h_{r1} = (h_{fMg} - h_{fM}) = +44$ (endothermic) $h_{r2} = (5.67h_{fG} + 0.41h_{fS} - h_{fW}) = -528$ (exothermic)	J/kmol
i	i^{th} species or i^{th} reaction	M, M_g, W, G, S,1, 2	None
k	Thermal conductivity	0.4	W m^{-1} K^{-1}
[M]	Adsorbed moisture concentration	Initially $\omega_M \times \rho_{bo}/M_{wM}$ or 1.44	$kmol/m^3$
[M_g]	Desorbed moisture concentration	Initially 0	$kmol/m^3$
M_{wi} where i = M, M_g, W, G, S	Molecular weight of i^{th} species	18.0, 18.0, 186.5, 24.3, 105.8	kg $kmol^{-1}$
n	Pressure exponent	5.4	None
norminv	Inverse of the standard normal distribution	Function (see Microsoft Excel NORMINV)	None
P	Absolute pressure	Initially P_o	MPa
P_o	Initial pressure	0.083 (NM)	MPa
P_{fail}	Pore failure pressure	5	MPa
$\dot{q}_{decay}$	Decay energy	0.15	W
ρ	Density	Field variable	kg m^{-3}
ρ_{bo}	Initial bulk density	785	kg m^{-3}
ρ_c	Condensed density	Field variable	kg m^{-3}
ρ_{co}	Initial condensed density	1394	kg m^{-3}
R	Gas constant	8314	m^3 Pa K^{-1} $kmol^{-1}$
[S]	Solid concentration	Initially 0	$kmol/m^3$
S_f	Solid fraction	$S_f = (Mw_M[\mathrm{M}] + Mw_W[\mathrm{W}] + Mw_S[\mathrm{S}] +)/\rho_{bo}$	kg/kg
t	Time	Global variable	S
T	Temperature	Field variable	K
[W]	Waste concentration	Initially $\omega_{waste} \times \rho_{bo}/M_{wW}$ or 4.07	$kmol/m^3$
T_o	Initial temperature	LANL Drums A, B: 298 LANL Drum C: 289 LANL Drum D: 292 Drum 68660: 264	K
V_{ex}	Extra gas volume (*i.e.*, trash void and headspace	0.112	m^3
$V_{o,W}$	Initial volume of waste	0.054	m^3
ω_{H2O}	Mass fraction of adsorbed water [10]	0.033	kg/kg
ω_W	Mass fraction of waste [10]	0.967	kg/kg
ξ	norminv: inverse of the standard normal distribution	Field variable	None
ξ_1	norminv for 1st reaction	Field variable	None

The micromechanics model uses an analytical solution of the spherical elastic equations for compressibility and thermal expansion to describe internal pressurization caused by both temperature and decomposition occurring within closed pores of the waste. Parameters used for the micromechanics model are found in [13].

8.2 Model Predictions

Model predictions were compared to the four LANL drum tests in Figure 4-1 and Drum 68660 in Figure 4-3. In this section, model predictions are compared to two small scale experiments at both SNL and PNNL.

The SITI experiment confines the vented waste in a 2.54 cm diameter by 2.54 cm tall cylinder with machined expansion gaps as shown in Figure 8-1(a-b). Internal temperatures were measured at the thermocouple locations shown in Figure 8-1(c). Figure 8-1 (d) shows a picture of one of the six different LANL surrogate wastes (LANL WB4) [12] used in the SITI experiments which is heated linearly using rope heaters at about 5 °C/m. The measured internal temperature for six different wastes with varying amounts of nitrate salts are shown in Figure 8-1(e). The predicted center temperature for these waste surrogates is shown in Figure 8-1(e) as a bold black line. The predicted ignition time was 1294 s which corresponds to the measured exotherm for all six of the surrogate waste experiments. More details regarding the SITI apparatus and waste surrogates can be found in [10].

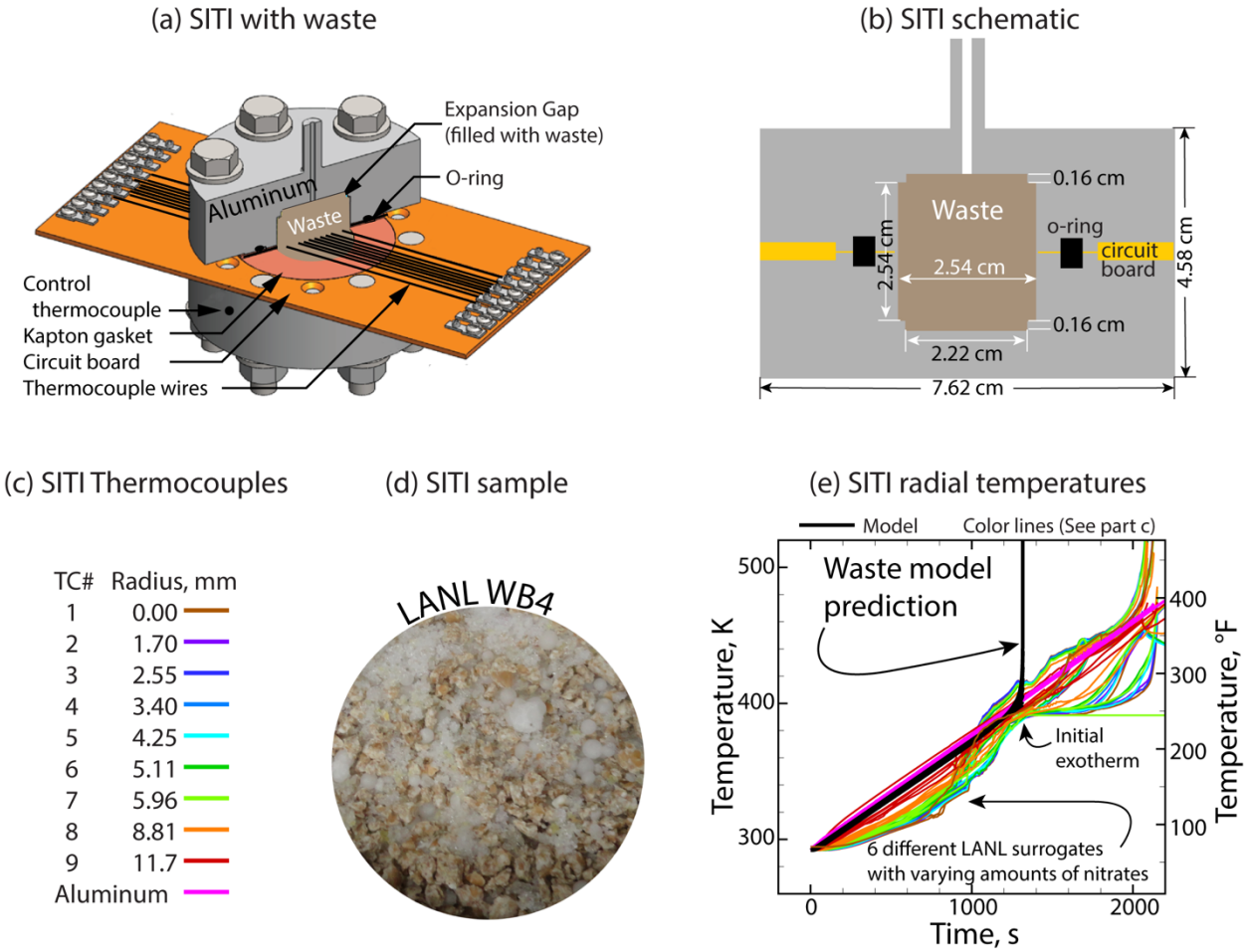

Figure 8-1. (a,b) SITI schematics, (c) thermocouple bead locations, (d) waste picture, and (e) SITI radial temperature profiles corresponding to 5 different LANL waste surrogates with varying nitrate amounts. The Waste model prediction (black line) corresponds to the initial exotherm in the waste surrogates.

Thermal ignition was observed in two ARC experiments at PNNL [38][39]. The sWheat Scoop®/nitric acid waste sample was placed in closed spherical vessels made of titanium with an internal volume of 9.5 cm^3 and working pressure of 20 MPa (2900 psi). The samples were heated using a heat/wait/search mode. The primary difference between the two ARC experiments was that one contained 7.5 g of dried 3.5 M nitric acid saturated sWheat Scoop® [10] and the other contained 6.9 g of dried 3.5 M nitric acid saturated sWheat Scoop® [38]. The difference in sample size makes a slight difference in the available gas volume within the sample vessels. The ignition occurred in the two samples when the sample temperature reached 346 K (163 °F) and 351 K (172 °F). Figure 8-2 (a) shows 5 ARC simulations with the temperature ramped from 293 K (68 °F) at five heating rates of 1, 2, 3, 4, and 5 K/min. Constant rate boundary conditions were used due to lack of temperature information on the heat/wait/search mode. The gray box in Figure 8-2 (a) bounds the measured ignition time that corresponds to the sample reaching 346 K (163 °F) and 351 K (172 °F), respectively. Figure 8-2 (b) shows the ARC sample containers after each of the experiments.

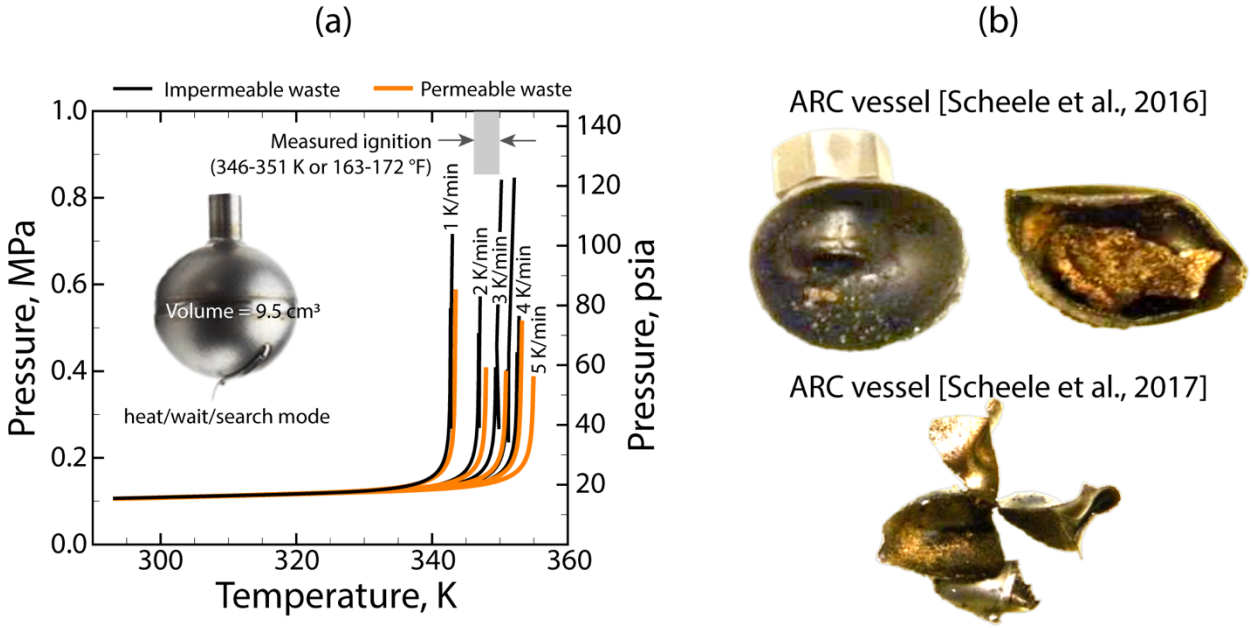

Figure 8-2. (a) Predicted radial temperatures and pressures in ARC calorimeter containing surrogate waste heated at 5 °C/min. The inset photo shows a picture of a new sample vessel. The pictures in (b) show the sample vessel after ignition.

8.3 Uncertainty Analysis

Uncertainty in the model predictions was determined using a Latin Hypercube Sampling (LHS) analysis, which is based on a Latin square design. Input parameters are randomly selected from equal probability bins to avoid concentration about the mean. This technique allows input uncertainty to be efficiently propagated into model predictions [40]. Input parameters that contribute the most to the output uncertainty have a high correlation coefficient with the output parameters. Absolute Pearson correlation [41] coefficients above 0.3 significantly influence model predictions such as ignition time or internal temperature profiles.

Nine model parameters used in a 20 sample LHS analysis are presented in Table 8-2. Table 8-3 presents 20 LHS samples with predicted ignition times for Drum 68660 being 40±0.6 days (impermeable waste) and 64±2 days (permeable waste). The uncertainty input parameter ranges in Table 8-2 are assumed to be distributed uniformly about the mean value. Uncertainty in the reaction mechanism is accounted for by using a rate multiplier as well as specifying uncertainty in the reaction enthalpies. Uncertainty in thermophysical properties, such as the thermal diffusivity, are accounted for by the uncertainty in thermal

conductivity and specific heat. Uncertainty in the initial density, radiation source, gas ullage volume, and moisture content are also included in the analysis.

The most important input parameters that contribute to the uncertainty predictions are correlated. Lack of correlation supports the hypothesis that changes in the input parameter, at least over the range in Table 8-2, do not appreciably change the predicted ignition time. The most important parameters affecting the uncertainty in the predictions with the impermeable bed are the initial bulk density and the moisture mass fraction. The most important parameters affecting the uncertainty in the permeable bed predictions are the bulk density, the headspace volume, the moisture mass fraction, and the rate multiplier.

Table 8-2. Parameters in LHS sensitivity analysis

#	Symbol	Description	Range	mean	r for 68660 impermeable	r for 68660 permeable
1	$C_{p,273}$	Specific heat at 273 K, J/kgK	1090-1210	1150	0.12	0.01
2	$C_{p,343}$	Specific heat at 343 K, J/kgK	1490-1650	1570	0.09	0.07
3	k	Thermal conductivity, W/mK	0.2-0.6	0.4	-0.16	0.04
4*	ρ_{bo}	Bulk density, kg/m^3	745-825	785	-0.84*	-0.66*
5	$\dot{q}_{decay}$	Radiation source, W	0.12-0.18	0.15	0.05	-0.04
6	V_{ex}	Excess vol. (i.e, headspace), m^3	0.10-0.12	0.11	0.03	0.59*
7*	U_{hrxn}	Heat of reaction multiplier	0.95-1.05	1	0.06	0.04
8*	ω_{h2o}	Moisture mass fraction	0-0.066	0.033	-0.51*	-0.31*
9*	X	rate reduction factor	0.95-1.05	1	-0.21	-0.35*

*Most important input parameters affecting the uncertainty in the predicted ignition times.

Table 8-3. LHS runs used to determine sensitivity of ignition time to parameter variations.

										Drum 68660 ignition time, days		
LHS runs	$C_{p,273}$	$C_{p,343}$	k	ρ_{bo}	q_{decay}	V_{ex}	U_{hrxn}	ω_{h2o}	X	Impermeable	Permeable	
1	1120.2	1538.9	0.563	816.2	0.137	0.1190	0.9790	0.0624	0.963	39.21	64.14	
2	1141.4	1505.1	0.552	801.2	0.138	0.1189	1.0087	0.0082	1.011	39.83	64.70	
3	1127.2	1522.1	0.383	787.1	0.180	0.1114	0.9728	0.0242	1.035	39.82	62.56	
4	1167.8	1642.4	0.236	768.3	0.173	0.1144	1.0285	0.0300	1.005	40.48	64.70	
5	1190.5	1549.2	0.254	784.3	0.122	0.1137	1.0034	0.0488	0.995	40.10	64.18	
6	1153.6	1532.3	0.460	764.6	0.145	0.1022	1.0140	0.0576	1.033	39.92	61.68	
7	1137.0	1496.0	0.307	745.1	0.161	0.1154	1.0496	0.0281	0.955	41.32	68.17	
8	1201.9	1632.7	0.466	769.1	0.124	0.1073	0.9616	0.0190	0.984	40.64	65.06	
9	1095.6	1625.7	0.369	779.0	0.134	0.1168	1.0398	0.0519	1.029	39.76	63.86	
10	1147.2	1639.8	0.354	759.8	0.167	0.1175	0.9667	0.0222	0.992	40.81	66.83	
11	1115.1	1514.2	0.213	792.6	0.155	0.1086	0.9519	0.0393	1.042	39.78	61.21	
12	1194.2	1513.7	0.437	756.2	0.157	0.1038	0.9809	0.0110	1.015	40.74	63.88	
13	1108.8	1614.5	0.515	807.6	0.163	0.1090	0.9562	0.0144	1.002	39.78	62.57	
14	1204.9	1592.5	0.494	795.4	0.175	0.1102	0.9906	0.0652	0.967	39.66	63.24	
15	1101.3	1568.5	0.289	812.6	0.130	0.1010	0.9897	0.0455	0.958	39.71	61.33	
16	1170.8	1609.0	0.327	819.9	0.142	0.1054	1.0349	0.0029	0.988	40.04	62.08	
17	1161.7	1575.3	0.415	776.6	0.128	0.1125	0.9955	0.0047	1.022	40.47	64.72	
18	1177.9	1583.0	0.536	800.9	0.148	0.1069	1.0432	0.0404	1.046	39.32	60.69	
19	1103.9	1601.3	0.587	752.2	0.151	0.1005	1.0199	0.0337	0.971	40.73	64.26	
20	1185.5	1556.4	0.279	821.4	0.170	0.1048	1.0229	0.0544	0.977	39.40	60.60	
ave.	1150.33	1570.62	0.40	785.51	0.15	0.11	1.00	0.033	1.000	40.08	63.52	ave.
r_i*	0.12	0.09	-0.16	-0.84	0.05	0.03	0.06	-0.51	-0.21	0.57	1.98	st.dev.
r_p*	0.01	0.07	0.04	-0.66	-0.04	0.59	0.04	-0.31	-0.35			

*r_i and r_p are the Pearson correlation coefficients for impermeable and permeable predictions, respectively.

Figure 8-3(a) shows the predicted temperatures near the edge of the waste for the 20 LHS simulations using the impermeable bed assumption where the ignition occurs near the edge of the waste. Figure 8-3(a) also shows the predicted center temperatures for the permeable bed calculations. Longer ignition times cause the ignition location to be deeper into the bed. Figure 8-3(b) shows the pressures predicted on the edge of the bed for all LHS calculations.

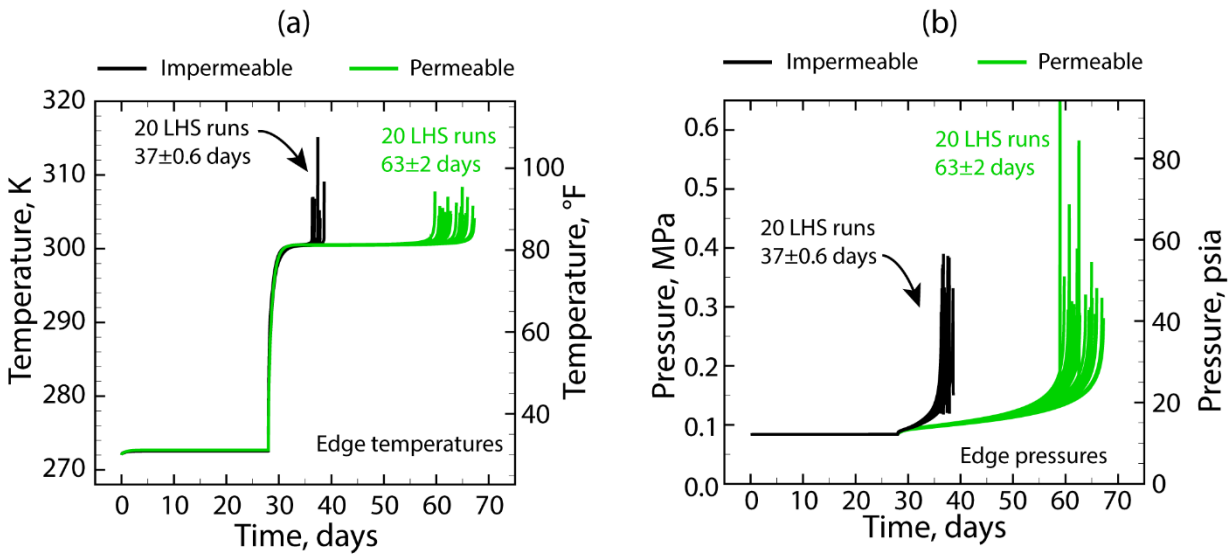

Figure 8-3. Predicted (a) temperatures and (b) pressures for each of the LHS runs.

Figure 8-4 and Figure 8-5 present plots of the ignition time with the input parameters listed in Table 8-2 and Table 8-3 that correlate to the predicted ignition time. Figure 8-4 shows correlation for the predictions that assume the bed is impermeable. Figure 8-5 shows correlation for the predictions that assume the bed is permeable. Trends are as expected, e.g., ignition time increases with larger headspace volume.

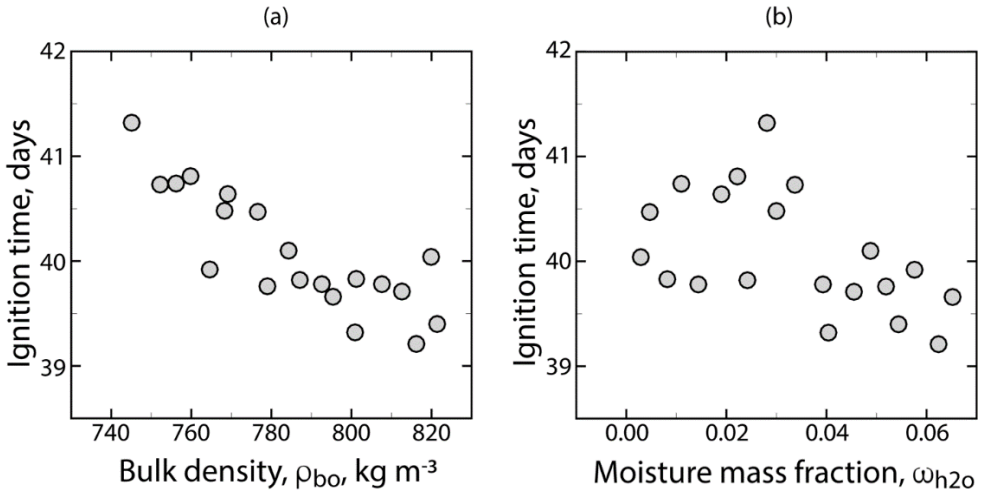

Figure 8-4. Sensitivity of predicted ignition time with (a) bulk density and (b) moisture mass fraction when the bed is impermeable.

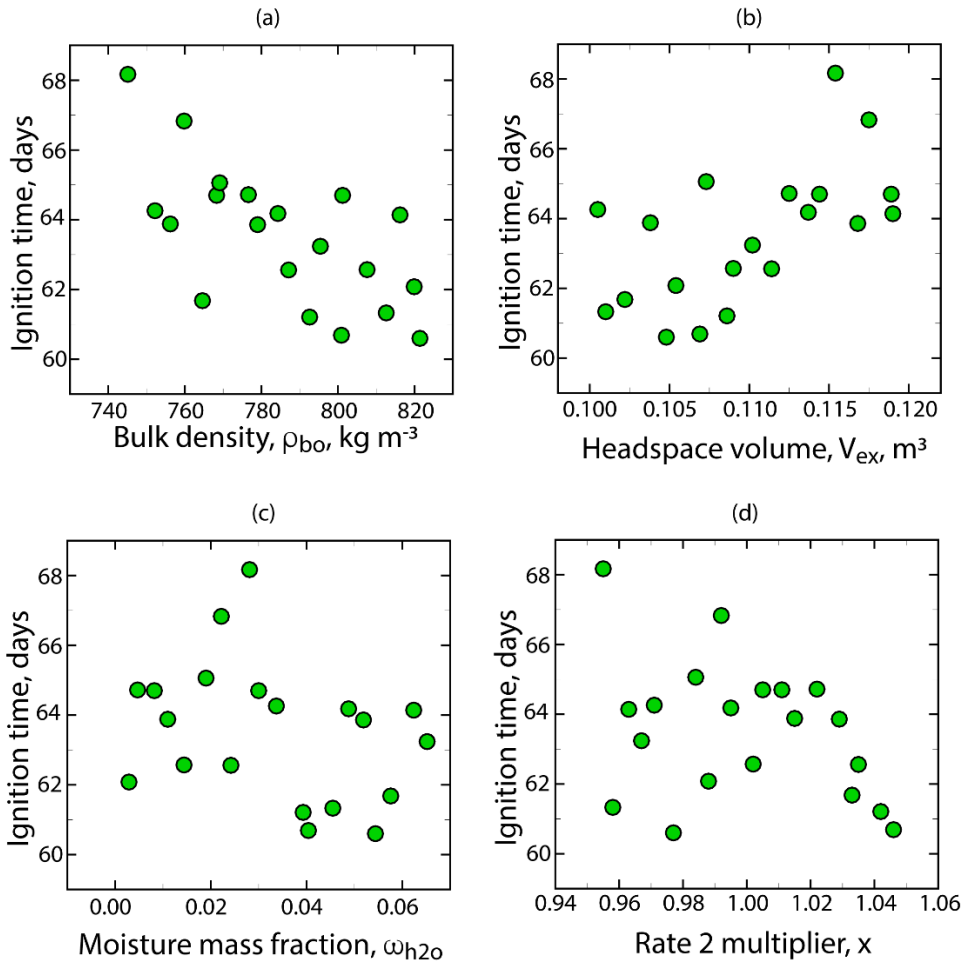

Figure 8-5. Sensitivity of predicted ignition time with (a) bulk density, (b) head space volume, (c) moisture mass fraction, and (d) reaction rate 2 when the bed is permeable.

9.0 Appendix. Nitric Acid – Carbohydrate Reactions

9.1 Oxidation of Carbohydrates by Nitric Acid

The section that follows discusses nitric acid chemistry and nitric acid oxidation of the key functional groups in carbohydrates and their oxidation products, i.e., alcohols, aldehydes and carboxylic acids. The origin of the autocatalytic reaction is discussed and how the interconversion of nitrogen oxide species is key to sustaining the oxidation reactions.

Nitric acid is a common oxidizing agent that is widely used in industry for oxidation of organic and inorganic compounds [25][42][43]. Nitric acid can also serve as a nitrating agent, typically when mixed with a dehydrating agent like sulfuric acid to generate NO_2^+ [44]. Many (but not all) nitric acid oxidation reactions are autocatalytic in which there is an induction period followed by an exothermic reaction with rapid product evolution and heat generation. In some cases, these oxidation reactions have led to runaway reactions and explosions [24].

The mechanisms for oxidation reactions by nitric acid are complex. Reactivity of the matrix depends on many factors including concentration of the nitric acid, concentration of the substrate, temperature, and any additional additives, such as acids, nitrite ions, or metal ions. In general, nitric acid rarely oxidizes organic compounds directly, but instead forms reduced nitrogen oxide species, such as NO_2 and HNO_2, which react

with the organic compounds [25]. Many of the nitrogen species that form are gaseous, and their concentrations in solution are dependent on their solubility, reactivity, concentration of nitric acid, and temperature.

Using data from the literature and nitrous acid analysis, researchers [29] developed a model to determine the concentration of different aqueous nitrogen species present in pure nitric acid for an acidity range of 1.5 – 8.5 M and temperatures ranging from 323-368 K. The most concentrated species at 323 K, after nitrate (NO_3^-) and nitric acid (since dissociation is incomplete over 10^{-2} M), is nitric oxide (NO, 10^{-4} M), followed by nitrous acid (HNO_2, 10^{-5} M), nitrogen dioxide (NO_2, 10^{-8} M), nitronium ion (NO_2^+, 10^{-7} –10^{-10} M) and nitrosonium ion (NO^+, 10^{-14} – 10^{-15} M).

The concentrations of these species change with acidity and temperature and are limited by their solubilities. For example, the solubility of NO in water at 298 K is 1.94 x 10^{-3} M L^{-1} atm^{-1} [45]. NO_2 reacts with water to form nitric acid (reaction B.1, 1 x 10^8 $M^{-1}s^{-1}$) based on its solubility in water, 7 x 10^{-3} M at^{-1} at 295 K (i.e., Henry's law coefficient, which is the partial pressure of NO_2 in the air vs concentration in water) [26].

$$3NO_2(g) + H_2O\ (l) \longrightarrow 2HNO_3\ (l) + NO\ (g) \quad \text{(B.1)}$$

Concentrated nitric acid solutions (15.7 M, 70%) can undergo self-ionization by dehydration to nitrogen pentoxide (reaction B.2), which is completely dissociated in nitric acid solutions into nitronium and nitrate ions (reaction B.3) [46].

$$2HNO_3 \rightleftharpoons N_2O_5 + H_2O \ \text{(self-ionization)} \quad \text{(B.2)}$$

$$N_2O_5 \rightleftharpoons NO_2^+ + NO_3^- \ \text{(complete dissociation)} \quad \text{(B.3)}$$

In the liquid and gas phase, nitric acid can slowly undergo thermal decomposition at room temperature (or photochemical decomposition) to nitrogen dioxide (reaction B.4) with fast equilibrium to dinitrogen tetroxide (reaction B.5), which leads to yellow or even red colored solutions at higher temperatures. In the gas phase, nitrogen dioxide is in fast equilibrium with nitric oxide (reaction B.6).

$$4HNO_3 \rightleftharpoons 4NO_2 + 2H_2O + O_2 \quad \text{(B.4)}$$

$$2NO_2 \rightleftharpoons N_2O_4 \ \text{(liquid phase)} \quad \text{(B.5)}$$

$$2NO_2 \rightleftharpoons 2NO + O_2 \ \text{(gas phase)} \quad \text{(B.6)}$$

In the RNS drums, the nitric acid can react with the sWheat Scoop®, which is primarily composed of starch, a branched polysaccharide composed of α–glucose units. The most reactive functional group in starch is the alcohol units (-OH). When nitric acid concentrations are >1M, the autocatalytic oxidation of alcohols, aldehydes, ketones and carboxylic acids, as well as the oxidation of inorganic species, such as arsenite, ferrous ion, thiocyanate, hydroxylamine, bromine, sulfite, and vanadium (V) has an induction period followed by an exothermic reaction with rapid product evolution and heat generation [27].

It has been determined that HNO_2 is the key reagent in the autocatalytic reaction [25][27][28]. In most oxidation mechanisms, the first step is the formation of nitrogen dioxide from nitric acid and nitrous acid (see reactions B.7 and B.8) [27]. Although the concentration of nitrous acid is very low in nitric acid [29], it has been shown that seemingly insignificant concentrations of nitrous acid, 10^{-7} to 10^{-4} M, influence the induction period of the oxidation reaction [27].

$$HNO_3 + HNO_2 \rightleftharpoons N_2O_4 + H_2O \quad \text{(B.7)}$$

$$N_2O_4 \rightleftharpoons 2NO_2 \quad \text{(B.8)}$$

Moreover, the induction time can be shortened by the addition of nitrite ions (NO_2^-) or nitrous acid (HNO_2) or lengthened by the addition of nitrite scavengers, such as urea, azide or hydrazine and at high concentrations, scavengers inhibit the reaction [27][30]. Acidity has also been shown to be important in the oxidation of benzyl alcohols and benzyl methyl ethers [31][47][48] and in many other reactions. In fact, the autocatalytic reaction is shut down below 2.5M HNO_3 for some reactions which highlights the importance of acidity on the nitric acid equilibria with the nitrogen oxide species [27].

The nitric acid oxidation of alcohols is autocatalytic because two moles of nitrous acid are produced (reaction B.9) for every mole consumed (reaction B.7) which leads to additional exothermic oxidation reactions and thermal runaway [25][27][31].

$$RCH_2OH + HNO_2 + HNO_3 \rightleftharpoons RCHO + 2HNO_2 + H_2O \quad (B.9)$$

To understand how this happens, it is important to identify the reaction mechanisms and the intermediates involved in the oxidation of alcohols by nitric acid. In general, NO^+ is the key reactive species in the oxidation of alcohols which is formed by disproportionation of NO_2 (reaction B.10) and by hydrolysis of HNO_2 (reactions B.11). The NO^+ can react with an aliphatic alcohol to form an alkyl nitrite (reaction B.12) which cleaves to form either an aldehyde or ketone and HNO (reaction B.13).

The electrophilic mechanism is favored over the radical mechanism, i.e., hydrogen abstraction by NO_2 since the rate of oxidation of substituted benzyl alcohols increased with electron donating substituents and the Hammett plot showed a negative slope, indicating a positive charge in the transition state [48]. However, N_2O_4 has also been proposed as the reactive species in the oxidation of formaldehyde monohydrate ($CH_2(OH)_2$) in which a bimolecular reaction generates 2 moles of HNO_2 for every mole of product [28].

$$2NO_2 \rightleftharpoons NO^+ + NO_3^- \quad (B.10)$$

$$H^+ + HNO_2 \rightleftharpoons NO^+ + H_2O \quad (B.11)$$

$$RCH_2OH + NO^+ \rightleftharpoons RCH_2ONO + H^+ \quad (B.12)$$

$$RCH_2ONO \longrightarrow RCHO + HNO \quad (B.13)$$

In the oxidation of alcohols when the moles of acid are in excess to the moles of alcohol, i.e., fuel lean conditions, the reactive nitrogen dioxide radical (NO_2) can abstract hydrogen from nitroxyl to form nitrous acid and NO (reaction B.14). The NO can be oxidized by oxygen in the air to regenerate the nitrogen dioxide (reaction B.15) and continue the reaction. Thus, fuel lean reaction conditions promote autocatalytic reactions.

$$HNO + NO_2 \rightleftharpoons NO + HNO_2 \quad (B.14)$$

$$2NO + O_2 \rightleftharpoons 2NO_2 \quad (B.15)$$

For the converse case where the moles of alcohol are in excess to the moles of acid, i.e., fuel rich environments, the nitroxyl (HNO) formed in reaction B.13 can dimerize and form nitrous oxide (N_2O) (reaction B.16). In this case, the reaction will not be autocatalytic because N_2O is relatively inert at room temperature and HNO_2 is consumed in the reaction (reaction 7). Thus, the overall oxidation reaction under fuel rich environments is shown in reaction B.17 [49].

$$2HNO \longrightarrow N_2O + H_2O \quad (B.16)$$

$$2RCH_2OH + 2HNO_2 \rightleftharpoons 2RCHO + N_2O + 3H_2O \quad (B.17)$$

The RNS drums at LANL were observed to evolve CO_2 and N_2O, in addition to other gases, which is consistent with nitric acid oxidation of organics in a fuel rich environment. In Drum 68660, the organics are estimated to be in molar excess of the nitric acid (i.e., fuel rich) assuming a homogeneous mixture. Specifically, the remediated salt layer was estimated to contain 11.72 kg of sWheat Scoop® (mixed in a volume ratio of 0.7:1 with nitrate salts) and 0.40 kg HNO_3 which would provide a mole ratio of organics:nitric acid = 11.5 [10]. In the remediated liquid layer of Drum 68660, it was estimated that there was 12.26 kg of sWheat Scoop® and 1.57 kg of nitric acid which was neutralized with triethanolamine (KolorSafe®) [10]. If it is assumed that none of acid was neutralized, the ratio of organics:nitric acid = 3.1.

Nitric oxide (NO) can also produce nitrous acid by (rapid) oxidation with nitric acid (reaction B.18) [31], and by reaction with nitrogen dioxide (reactions B.19 and B.20). These reactions generate additional nitrous acid which promotes the autocatalytic oxidation of alcohols.

$$2NO + HNO_3 + H_2O \rightleftharpoons 3HNO_2 \quad \text{(B.18)}$$

$$NO + NO_2 \rightleftharpoons N_2O_3 \quad \text{(B.19)}$$

$$N_2O_3 + H_2O \rightleftharpoons 2HNO_2 \quad \text{(B.20)}$$

Although the initial product from the oxidation of an alcohol is an aldehyde or ketone, these products can be further oxidized by nitric acid, in exothermic reactions, to carboxylic acids and carbon dioxide. For example, formaldehyde can be oxidized to formic acid (reaction B.21) and then to carbon dioxide (reaction B.22) [28][50]. Aliphatic alcohols, such as decanol, octanol and hexanol, have been oxidized to the corresponding carboxylic acid in high yields (>80%) at 298 K with 80% nitric acid [51]. For these reactions to occur, it was found that the nitric acid concentration needed to be 30% or greater.

$$CH_2O + HNO_3 \rightleftharpoons HCOOH + HNO_2 \quad \text{(B.21)}$$

$$HCOOH + HNO_3 \rightleftharpoons CO_2 + HNO_2 + H_2O \quad \text{(B.22)}$$

Some of the RNS drums contain oxalic acid, which was used to precipitate plutonium (IV) as the plutonium oxalate hexahydrate. Oxalic acid can also be oxidized by nitric acid to generate CO_2 (reaction B.23) [52].

$$3(COOH)_2 + 2\,HNO_3 \rightleftharpoons 6CO_2 + 2NO + 4H_2O \quad \text{(B.23)}$$

For carbohydrate polymers, such as starch and cellulose, nitric acid oxidizes the alcohol groups and depolymerizes the polymer through hydrolysis of the glycosidic linkages. Typically, depolymerization of starch is carried out in dilute acid solution (0.5 N) by a variety of acids, including nitric, hydrochloric, phosphoric, and sulfuric acid, to produce lower molecular weight products and glucose [53].

Cellulose, a carbohydrate composed of glucose, is oxidized on an industrial scale with concentrated nitric acid (sometime with nitrite ions as an initiator) to produce polyglucuronic acid [43]. This process oxidizes the hydroxyl group in the C6 position of glucose to the carboxylic acid. The monosaccharide, glucose, can be oxidized in a highly exothermic reaction with concentrated nitric acid to glucaric acid (i.e., the dicarboxylic acid) [54]. Sugar has also been used to consume nitric acid from synthetic Purex waste in which 19-22 moles of nitric acid were consumed per mole of sugar at 373 K in 12 h [55].

It has been reported that oxidized cellulose and lower molecular weight carbohydrates are more reactive than the high molecular weight, crystalline polysaccharides [22]. In the LANL RNS drums, the temperature dependent evolution of CO_2 and N_2O is consistent with nitric acid oxidation of organics in a fuel rich environment. It could be hypothesized that as nitric acid breaks down sWheat Scoop® into smaller, more reactive molecules, the rate of oxidation could accelerate because of increased mobility and reactivity of the constituents. However, this does not mean a thermal runaway reaction will occur.

From the discussion above, an autocatalytic oxidation reaction needs concentrations of nitric acid high enough to support the generation of the key reduced nitrogen oxide species required for the reactions (HNO_2, NO_2, NO^+, and NO), and with the limited solubilities of the nitrogen oxides, the gaseous nitrogen oxide species need to be kept from escaping the drum to support the feedback mechanism leading to an autocatalytic exothermic reaction. Also, the rate of heat generation must exceed the rate of heat dissipation so that the temperature of the reaction mixture increases (self-heating) and promotes additional exothermic reaction pathways [18]. Venting prevents volatile reactive species from building up and continuing to react while providing a route for dissipating excess heat through evaporation of water and volatile species, as demonstrated in drum-scale testing [11].

It is anticipated that the LANL RNS waste drums at WCS have been undergoing slow oxidation reactions and radiolysis over the last eight years, which produce gaseous products [3] similar to the 56 LANL RNS drums that were reprocessed [7]. For the LANL RNS waste, the rate of CO_2 and N_2O generation from the SWB and drums was temperature dependent, as higher concentrations of CO_2 and other gases were observed in the summer and lower concentrations in the winter.

LANL modeled this headspace gas behavior assuming a single reaction was responsible for generation of CO_2 and N_2O and an activation energy of 15-20 Kcal/mol was determined [36]. The estimated level of reactivity implied that it would take decades to consume all the organics in the drums assuming a single reaction. For example, based on the predicted total amount of CO_2 generated over 260 days for drum 68685 (the sibling to 68660), only 1 kg of sWheat Scoop® would be consumed within that timeframe, which is a very small fraction of the total amount of sWheat Scoop® available for reaction (>44 kg in 68685) [10][36]. Moreover, for all the RNS drums in storage at LANL, the concentration of these gases has decreased with time, indicating a decrease in reactivity and lower heat generations (since higher heat generation would increase gas production) [18].

The origin of the decrease in reactions could be from consumption of the reagents. Given that the 3.3M nitric acid was only present in the interstitial liquids of the salts in the RNS drums and sWheat Scoop® was added in excess (as discussed for 68660 above) at a recommended ratio of 3:1 sWheat Scoop®:unremediated nitrates , the nitric acid is the limiting reagent in the oxidation reaction [5]. Thus, as the nitric acid is depleted, both the rate of reaction, the volume of gases generated, and the heat generated decreases. Thus, the stability of the WCS RNS waste with respect to autocatalytic thermal runaway due to nitric acid chemistry should increase over time as the nitric acid is depleted from reactions in the drum.

10.0 Appendix. Drum, SWB, and MCC Configuration